

# COFs-Based Metal-Free Heterojunctions for Solar-to-Chemical Energy Conversion

Tianyu Zhou, Yunchao Ma, Hao Feng, Ye Lu, Guangbo Che,\* Chunbo Liu,\* and Yaqian Lan\*

Covalent organic frameworks (COFs) are a promising class of organic polymers with the merits of robust framework, ultrahigh porosity, and molecularly precise backbones, which reveals great potential for solar-to-chemical energy conversion in the context of mitigating energy and environmental crises. However, the photochemical activities of individual COFs are not as robust as desired, primarily due to their limited light absorption, insufficient dissociation of photogenerated excitons and readily recombined photogenerated carriers. Recently, COFs-based metal-free heterojunctions with synergistic effects provide a feasible route to boost the photocatalytic activity of COFs in more environmentally friendly and cost-competitive manners. Herein, it is first systematically overview the advances in COFs-based metal-free heterojunctions from heterojunction types, heterointerfaces interactions, and primary design mechanisms. Then, typical COFs-based metal-free heterojunction photocatalysts (e.g., g-C<sub>3</sub>N<sub>4</sub>-COFs, carbon materials-COFs, polymer semiconductor-COFs, COFs-COFs heterojunction) are summarized. Finally, the challenges and long-term outlooks for future advances of COFs-based metal-free heterojunction photocatalysts are offered from the terms of photocatalytic efficiency, yield, stability, cost and reaction mechanisms, as well as the standardized evaluation method of activities. It is anticipated that this review can deliver new insights into the fundamental and engineering of COFs-based metal-free heterojunctions for solar-to-chemical energy conversion, and further accelerate the development of this area.

environmental crises, which are in direct contradiction with the principles of sustainable development and raise significant concerns for human society.<sup>[1,2]</sup> Photocatalytic solar energy conversion is one of the minimal pollution and most promising solution to address aforementioned concerns, owing to the safety, cleanliness and inexhaustibility of solar energy.<sup>[3,4]</sup> Since the seminal work by Fujishima and Honda in 1972, who reported photoelectrochemical catalyzed H<sub>2</sub> production via TiO<sub>2</sub> semiconductor without the need for any external voltage,<sup>[5]</sup> photocatalytic energy conversion has garnering significant attention from the research community involving H<sub>2</sub> production, CO<sub>2</sub> reduction, pollutant degradation, H<sub>2</sub>O<sub>2</sub> production, antibacterial, nitrogen fixation, and high value-added chemical synthesis, etc.<sup>[6]</sup>

The long-standing objective of solar-to-chemical energy conversion requires discovering efficient and sustainable semiconductor photocatalysts possessing high solar responsiveness along with appropriate redox potentials. These catalysts should also contain abundant redox active sites for catalytic reactions while facilitating rapid mass transfer or adsorption processes. Additionally, they are expected to

be composed of environmental-friendly raw materials readily available within Earth's crust.<sup>[1,7]</sup> Decades of extensive and in-depth exploration on typical inorganic semiconductor photocatalysts (e.g., CdS, ZnO) have proved that tuning their properties

## 1. Introduction

The global industrialization, urbanization and extensive fossil fuel consumption inevitably give rise to energy shortages and

T. Zhou, Y. Ma, H. Feng, Y. Lu, C. Liu  
Key Laboratory of Preparation and Application of Environmental Friendly Materials, Ministry of Education  
Jilin Normal University  
Changchun 130103, P. R. China  
E-mail: [chunboliu@jlnu.edu.cn](mailto:chunboliu@jlnu.edu.cn)

T. Zhou, C. Liu  
Jilin Joint Technology Innovation Laboratory of Developing and Utilizing Materials of Reducing Pollution and Carbon Emissions  
College of Engineering, Jilin Normal University  
Siping 136000, P. R. China

G. Che  
Baicheng Normal University  
Baicheng 137000, P. R. China  
E-mail: [guangboche@jlnu.edu.cn](mailto:guangboche@jlnu.edu.cn)  
Y. Lan  
School of Chemistry  
South China Normal University  
Guangzhou, Guangdong 510006, P. R. China  
E-mail: [yqlan@m.scnu.edu.cn](mailto:yqlan@m.scnu.edu.cn)

 The ORCID identification number(s) for the author(s) of this article can be found under <https://doi.org/10.1002/adfm.202409396>

DOI: 10.1002/adfm.202409396

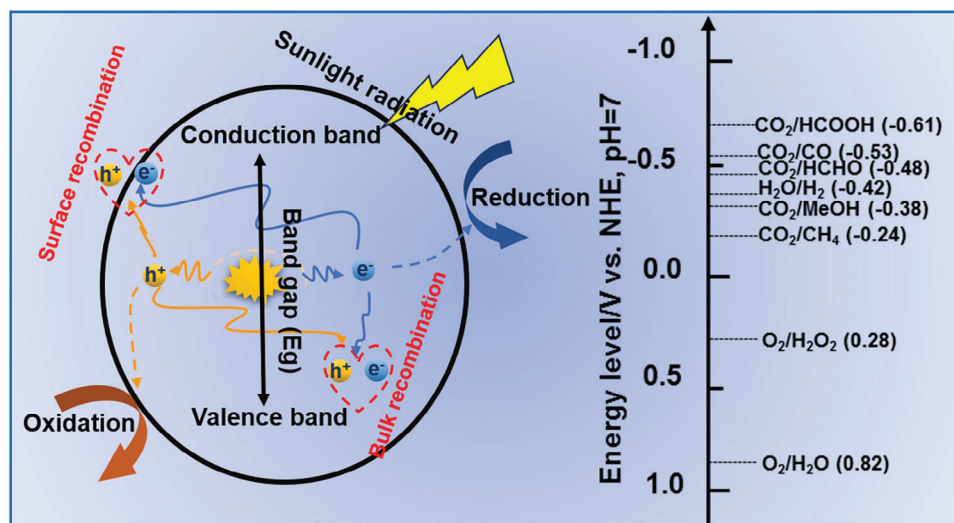


**Figure 1.** Schematic diagram of the basic principle and energy structure of photocatalytic oxidation-reduction reactions.

is challenging, while heavy metal leakage, photocorrosion and high cost have to face.<sup>[2,8,9]</sup> In contrast, the development of earth-abundant and light element based soft photocatalysis over recent decades has demonstrated its superiority in terms of affordability, reduced toxicity, tuneable electronic properties through molecular engineering, while as robust, stable and recoverable as their inorganic counterparts.<sup>[10,11]</sup>

Covalent organic frameworks (COFs) are a class of crystalline porous metal-free materials with designable knots and linkers periodically connected via covalent bonds, which are composed of light elements (C, N, O, B, etc.).<sup>[12,13]</sup> Since 2005, their discovery by Yaghi group,<sup>[14]</sup> various types of COFs have been extensively investigated, including boroxine, boronate ester, imine, azine,  $\beta$ -ketoenamine, triazine,  $sp^2$ -carbon linked COFs.<sup>[15]</sup> Due to the abundant designability of diverse organic monomers, the intrinsic regularity and orderliness of crystal structure, as well as the versatility of covalent bond formations, COFs possess incomparable merits over other traditional porous materials of metal organic frameworks, molecular sieves and porous polymers, and extensively apply in diverse fields such as energy storage,<sup>[12,16]</sup> adsorption/separation,<sup>[15,17]</sup> sensors/cancer-phototherapy,<sup>[18,19]</sup> photo/electrocatalysis.<sup>[5,20–24]</sup> Among them, the application of COFs in photocatalysis, based on some basic principles and energy structures<sup>[4]</sup> (Figure 1), is attracting particular attention due to diverse distinct features.<sup>[5,23,25]</sup> For instance, 1) Suitable pore size/distribution, larger surface area and swift reaction/adsorption/migration kinetics. Permanent porosity with uniformity pore size and distribution creates high specific surface area, which is beneficial for loading plentiful catalytic active sites and fully contacting with reactant molecules as well as migration of photogenerated charges.<sup>[8]</sup> 2) High physicochemical stability. The strong covalent bonds connecting various building blocks confer COFs with exceptional physicochemical stability in acidic, alkaline, and some redox environments to participate in catalytic reaction.<sup>[26]</sup> 3) Designability. Periodic structures allow facile atomic precision modification and functionalization that guide the growth of long-range ordered crystal structures through topological predesign,<sup>[27]</sup> thus fascinat-

ing to charge transfer, and aiding in understand the structure-function-activity relationships and further optimize the catalytic properties.<sup>[28]</sup>

Although numerous researches have confirmed the research value of COFs-photocatalysis and several excellent reviews have summarized the relevant progress,<sup>[5,23]</sup> they also highlighted certain limitations in this area. The primary challenges arise from limited light harvest, and the insufficient dissociation of photogenerated exciton in single COFs photocatalyst on account of their inherent low polarity, which restrict their broad applications.<sup>[1,29,30]</sup> Constructing heterostructures has proved to be a commendable strategy to conquer aforementioned challenges of COFs as it can promote the spatial separation of photogenerated charges through electronic band alignment while simultaneously harnessing the merits of each components.<sup>[31,32]</sup> Professor Lan's group designed a series of COF-semiconductor Z-scheme heterojunctions coupling  $CO_2$  reduction COFs (COF-316 and COF-318) with water oxidation metal semiconductors ( $\alpha$ - $Fe_2O_3$ ,  $TiO_2$  and  $Bi_2WO_6$ ), and realized efficient photocatalytic  $CO_2$ -to- $CO$  conversion with  $H_2O$  as the electron donor, no participation of photosensitizers, cocatalysts and sacrificial agents.<sup>[7]</sup> Recently, through the comparison of COFs with oxidation-reduction molecular junction<sup>[21,33,34]</sup> and some metal-free COFs researched by Lan' group and Liu' group,<sup>[35–37]</sup> we found that inadequate compatibility between metal and non-metal photocatalyst remains a challenge, particularly in terms of disturbed charge transfer caused by lattice mismatch and interatomic diffusion.<sup>[38]</sup> Furthermore, the starting materials of COFs usually high cost and require complex synthesis procedure. Meanwhile, most COFs heavily rely on metals (primarily precious metals) to achieve their exceptional photocatalytic activity, which further diminishes the economic value of COFs as photocatalysts.<sup>[8]</sup> The incorporation of metals not only escalates raw material expenses but also amplifies the risk of environmental pollution, thereby greatly impeding large-scale industrial applications.

As a typical type of metal-free material, COFs possess plentiful aromatic rings, which endows superior compatibility toward various organic materials, e.g., graphitic carbon nitride ( $g-C_3N_4$

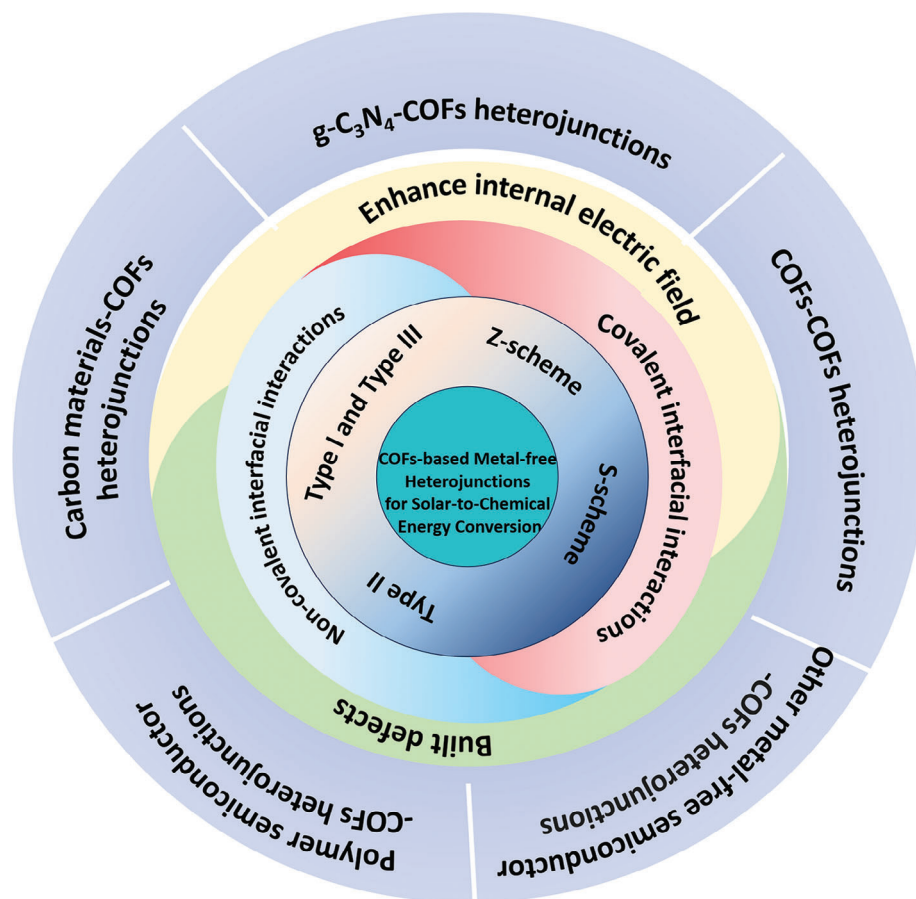


**Figure 2.** The overall structure schematic illustration of this review: heterojunction types, heterointerface interactions, design mechanisms, and typical COFs-based metal-free heterojunction photocatalysts.

or CN), graphene, through covalent bonds, van der Waals (VDW) forces,  $\pi$ - $\pi$  interactions, etc. In response to the growing demand for scalable and sustainable catalysis, COFs-based metal-free heterojunction photocatalysts are intensively investigated based on their merits, e.g., composition of earth abundant light elements, potential for reducing the cost of COFs photocatalysts, comparable activity to precious-metals COFs heterojunctions.<sup>[8,39]</sup> Up to now, there are numerous comprehensive reviews available summarizing typical structures and design of COFs-self,<sup>[40,41]</sup> application of COFs in different photocatalytic reactions,<sup>[42]</sup> various COFs-based inorganic or organic photocatalysts<sup>[1,3]</sup> or COFs-based composites.<sup>[43,44]</sup> Furthermore, considerable efforts also devoted to develop polymer/metal-free photocatalysts as a viable alternative to promote sustainable chemistry,<sup>[45,46]</sup> while there is no review exclusively focusing on COFs-based metal-free heterojunctions with a deep insight into this topic despite the increasing number of publications in this research area.

In this review, COFs-based metal-free heterojunction photocatalyst within the context of the current energy scarcity and environmental crisis are discussed for the first time. As depicted in **Figure 2**, first, heterojunctions types are introduced, while emphasis on direct Z-type and S-type heterojunctions. In addition, heterointerface interactions of COFs-based metal-free heterojunctions involving non-covalent interfacial interactions (VDW

forces, electrostatic interaction, hydrogen bonding, etc.) and covalent bonding (e.g., imine, amide, and C—O bonds) are summarized. Two primary strategies (enhance internal electric field and built defects) to create COFs-based metal-free heterojunction with efficient interface charge transfer are introduced. Then, typical COFs-based metal-free heterojunction photocatalysts (g-C<sub>3</sub>N<sub>4</sub>-COFs, carbon materials-COFs, polymer semiconductors-COFs, and so on) are summarized. Last but not least, challenges and long-term outlooks of COFs-based metal-free heterojunctions are elucidated, aiming at photocatalytic efficiency, yield, stability, cost, and reaction mechanisms, as well as the unstandardized evaluation method of activities. It is anticipated that this review can deliver new insights into the fundamental and engineering of COFs-based metal-free heterojunctions for solar-to-chemical energy conversion and further accelerate the development of this area.

## 2. Design of COFs-Based Metal-Free Heterojunctions

### 2.1. Heterojunction Types

As with other heterojunction, the reported COFs-based metal-free heterojunctions exhibit superior photocatalytic performance

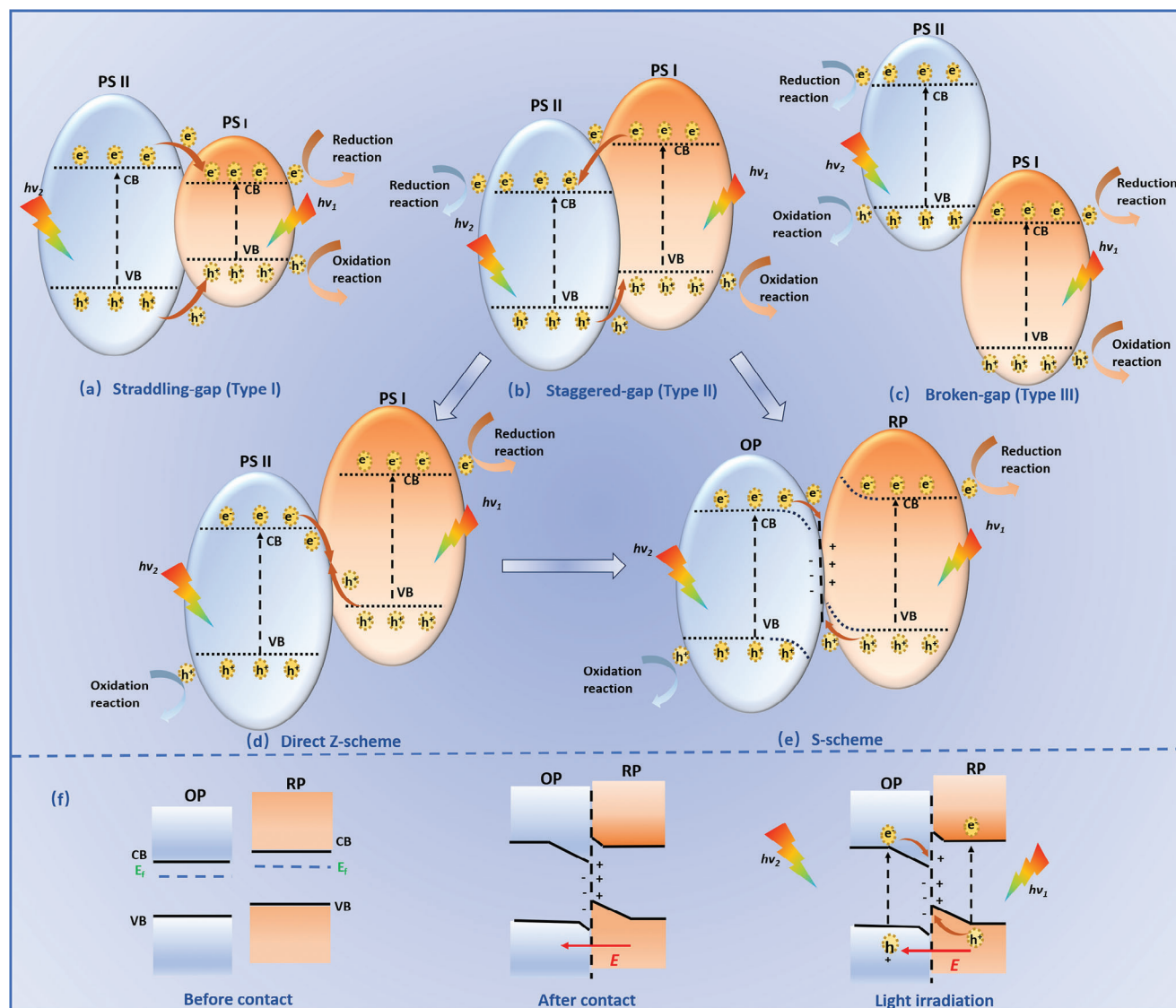


**Figure 3.** Band structures and charge transfer routes in Type I a), Type II b), Type III c), direct Z-scheme heterojunction d) and S-scheme heterojunction e). Detailed schematic diagram of charge transfer routes in S-scheme heterojunction f).

compared to single-component due to synergistic effects. Because in addition to the inherent advantages of COFs, the COF-based metal-free heterojunctions also demonstrate improvements in optics, conductivity, stability or cost-effectiveness. More importantly, the formation of heterojunctions improved charge behaviors in photocatalysis. Based on the conduction band (CB) and valence band (VB) relative positions of constituent photocatalysts (PS I and PS II), the heterostructures are categorized as straddling gap heterojunctions (Type I), staggered gap heterojunctions (Type II) and broken gap heterojunctions (Type III), along with derived Z-type and S-type heterojunctions,<sup>[1]</sup> as revealed in **Figure 3**.

In Type I heterojunctions (**Figure 3a**), the accumulation of electrons and holes predominantly occurs at the photocatalyst with a narrower band-gap (PS I), ultimately leading to an increased likelihood of recombination and causing poor photocat-

alytic activity.<sup>[1,47]</sup> In Type III heterojunctions (**Figure 3c**), both electrons and holes remain confined within their respective photocatalyst without undergoing mutual charge transfer, thereby resulting in the independent operation of the two photocatalysts without any synergistic effect.<sup>[1,47]</sup> In Type II heterojunctions (**Figure 3b**), the migration of electrons and holes to their individual low energy bands occurs, i.e., electrons preferentially gather in photocatalyst with lower CB (PS II) and holes tend to accumulate in photocatalyst with lower VB (PS I). Although the redox capacities diminish due to the localization of electron and hole within low energy potential, the photocatalytic activity can be improved due to carrier spatial separation.<sup>[39,47]</sup> Considering the diminished redox abilities of type-II heterojunction, Z-scheme heterojunction also with staggered band alignment (involving traditional liquid, all-solid-state and direct Z-scheme heterojunction) were proposed.<sup>[48]</sup> In direct Z-type heterojunctions (**Figure 3d**),

low-energy electron at the CB of PS II will transfer and then recombine with low-energy hole at the VB of PS I, leaving high-energy electron at the CB of PS I and high-energy hole at the VB of PS II for catalysis reaction. That is to say, direct Z-type heterojunctions not only achieve spatial separation of carrier, but also retain electron and hole with strong redox capacity to take part in catalytic reaction, thus achieving significant improvement in photocatalytic activity.<sup>[39,49]</sup>

To better integrate and explain the charge transfer mechanism of type-II heterojunctions and direct Z-scheme heterojunctions, step-scheme (S-scheme) heterojunctions (Figure 3e) with staggered gap is first brought forward by Yu and co-workers in 2019,<sup>[50,51]</sup> following a significant surge in the number of publications on S-scheme heterojunctions in recent years.<sup>[52–54]</sup> The S-scheme heterojunctions (Figure 3f) consists of an oxidation photocatalyst (OP) with a lower Fermi level and a reduction photocatalyst (RP) with a higher Fermi level. Upon contact, the electron in RP transfer toward OP at the interface, resulting in a positively charged RP side due to electron loss and a negatively charged OP side due to electron acceptance. Concurrently, at the RP-OP interface, band edge bend upward and downward due to the decreased and accumulation of electrons density, respectively.<sup>[39]</sup> Additionally, this process leads to the formation of a built-in electric field directed from RP to OP. Upon light irradiation, photogenerated electron will migrate from CB of OP to VB of RP, rapidly recombining through the three driving forces of Coulombic attraction, band bending, and built-in electric field. Conversely, the three driving forces also suppress the electron migrate from CB of RP to CB of OP and the hole migrate from VB of OP to VB of RP. Consequently, weak photogenerated carrier are effectively recombined, while high-energy photogenerated electrons and holes accumulate in the CB of RP and VB of OP, and the strong redox capacity is earned in the S-scheme heterojunctions.<sup>[39,49]</sup>

## 2.2. Heterointerface Interactions

A tightly contacted heterointerface with minimal charge transfer resistance is the fundamental prerequisite for fabricating high-quality COFs-based metal-free heterojunctions. In general, the heterointerfaces can be established via non-covalent interfacial interactions (VDW force, electrostatic interaction, hydrogen bonding, etc.) and covalent bonding (e.g., imine, amide and C-O bonds).<sup>[3]</sup> COFs-based metal-free heterojunctions based on non-covalent interactions are predominantly synthesized employing some mild methods likes self-assembly and grinding.<sup>[55]</sup>

VDW forces commonly exist between 2D atomic layers and typically results in a close interface between two photocatalysts (e.g., 2D COFs with 2D g-C<sub>3</sub>N<sub>4</sub> nanosheets, hexagonal boron nitride or graphene).<sup>[13,31,32]</sup> The formed 2D/2D COFs-based metal-free heterojunctions exhibit efficient interfacial charge mobility because of the larger face-to-face contact area and shorter migration distance.<sup>[56]</sup> Additionally, VDW heterojunction can overcome lattice match limitation and enable constructing strain-free and charge-free COFs-based metal-free heterojunctions with significantly boosted optical and electronic properties.<sup>[57]</sup> Through a facile and mild ultrasonication method, Zhu's group<sup>[56]</sup> constructed a 2D/2D VDW heterojunction with pre-synthesized CN and COF (Figure 4a). The synergistic effect of CN and COF me-

diated by VDW force promoted interfacial charges transfer and spatial separation, thereby significantly enhancing the photocatalytic hydrogen evolution (PHE) activity. When the weight ratio of COF was 12 wt.%, the COF/CN heterojunction exhibited an outstanding PHE activity of 449.64  $\mu\text{mol h}^{-1}$ , which is about fivefold higher than that of single components.

Coulomb electrostatic interaction utilizes two photocatalysts with opposite charges in solution to establish a closely connected interface through strong electrostatic attraction, which can be precisely regulated by the pH of solution.<sup>[49]</sup> Through a facile and environmental-friendly electrostatic self-assembly method (Figure 4b), Shang' group<sup>[32]</sup> fabricated a metal-free heterojunction photocatalyst by combining photo-reduced GO (PRGO, zeta potential of +8.4 mV) with sp<sup>2</sup>-carbon-chain triazine-based COF (TP-COF, zeta potential of -31.0 mV). The efficient dissociation of photogenerated charges was realized through the transfer of electrons from the CB of PRGO to the VB of TP-COF driven by energy band bending and built-in electric field. The constructed S-scheme heterojunction exhibited remarkable selectivity in gas-solid reducing CO<sub>2</sub> to CO without photosensitizers and sacrificial agents.

Hydrogen bonding can also create close contact interface, even forming low interfacial resistance and establishing an internal electric field between two catalysts.<sup>[58,59]</sup> Zhang et al.<sup>[59]</sup> built an intramolecular charge migration path through =C=O-H-N= hydrogen bonding between photosensitive donor-acceptor (D-A) COFs semiconductors and hydrophilic CDs, which extremely promoted the dissociation and migration of photogenerated charges confined in the  $\pi$ -orbitals of COFs (Figure 4c). Due to the hydrogen bonding interaction, the photogenerated electrons within the pores of COFs can be extracted by CDs and accumulated therein, producing plentiful reactive oxygen species ( $\bullet\text{OH}$ ,  $\bullet\text{O}_2^-$ , and  $^1\text{O}_2$ ) for synergistic sterilization. Through precise adjustment of CD dosage, the 4 wt.% CDs in COF@CD can realize excellent photocatalytic antibacterial activity (95%) even at a low level (50 mg mL<sup>-1</sup>) upon visible-light illumination for 1 h, and the survival rate against *E. coli* diminished 8.3 times in contrast to that of single COFs.

In contrast to the aforementioned non-covalent interfacial interactions, which may cause charge congestion at the contact interface and exhibit weaker physical interactions, covalent bonding provides a significantly tighter and more stable interface that effectively accelerates the interfacial carrier separation and migration.<sup>[47]</sup> COFs-based metal-free heterojunctions based on covalent bonding predominantly utilize in situ growth or post-modified synthesis through Schiff-base reaction, cyanide copolymerization, etc.<sup>[47]</sup> Typically, g-C<sub>3</sub>N<sub>4</sub> possesses plentiful terminal amino groups that can react with the aldehyde groups on COFs to generate imine bonds via Schiff-base reactions, thereby improving the migration of photogenerated charges.<sup>[27,39]</sup> Wang et al.<sup>[39]</sup> utilized a solvothermal method to in-situ grow a nitrogen-enriched COF TMP onto CN using three C3 symmetry monomers, namely melem, 1,3,5-triformyl phloroglucinol (TP) and 2,4,6-tris(4-aminophenyl)-1,3,5-triazine (TAPT) through Schiff-base linkage (Figure 5a). By exploiting the propelled intramolecular charge transfer effect resulting from the charge density disparity between TAPT and melem units within the TMP shell (electron transfer from TAPT to melem, Figure 5b), they successfully constructed a cocoon-like CN/TMP composite that

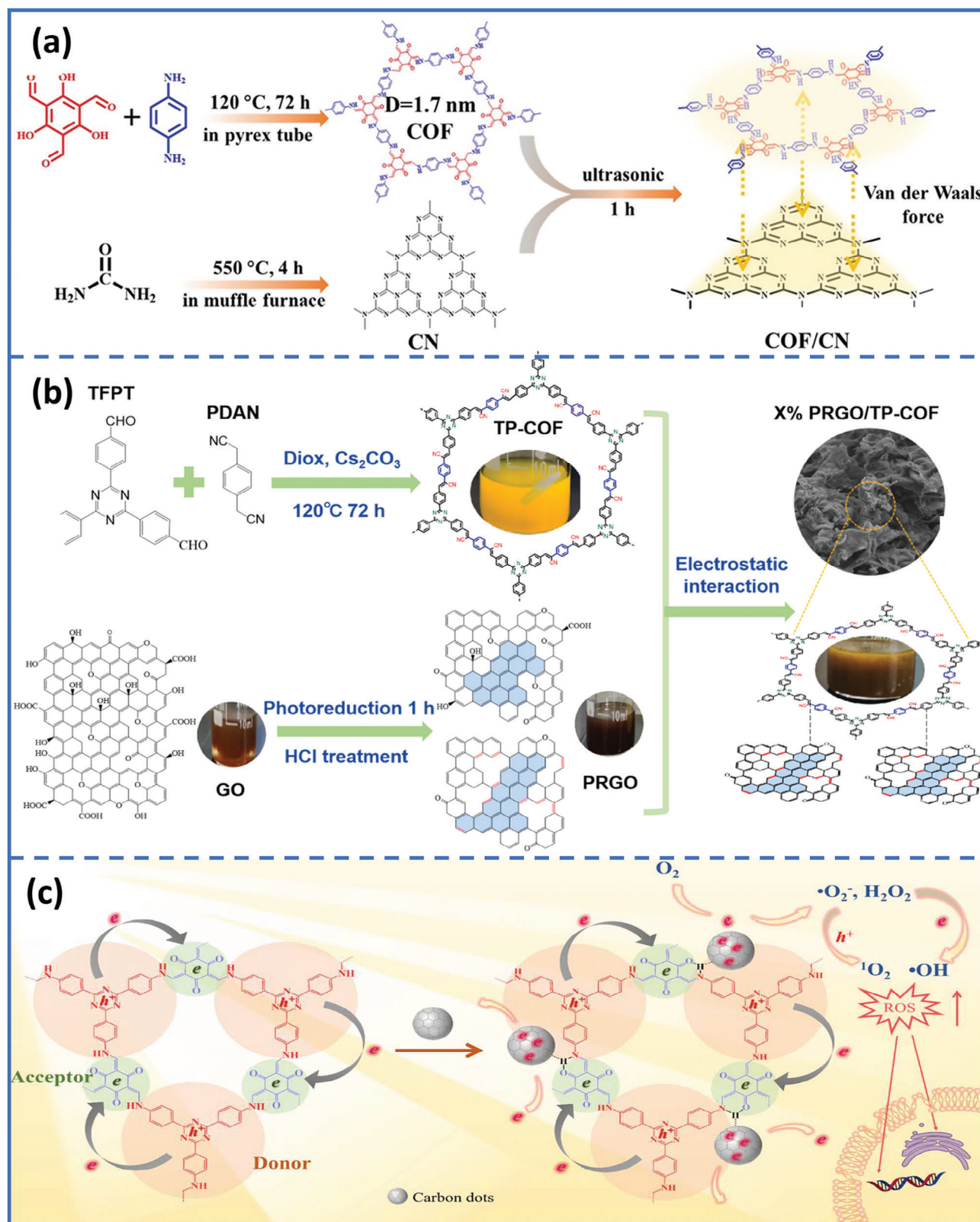


**Figure 4.** Constructing COFs-based metal-free heterojunctions based on non-covalent interfacial interactions. a) VDW force, reproduced with permission. Copyright 2023, American Chemical Society. b) Electrostatic interaction, reproduced with permission.<sup>[32]</sup> Copyright 2024, Elsevier. c) Hydrogen bonding, reproduced with permission.<sup>[59]</sup> Copyright 2022, The Royal Society of Chemistry.

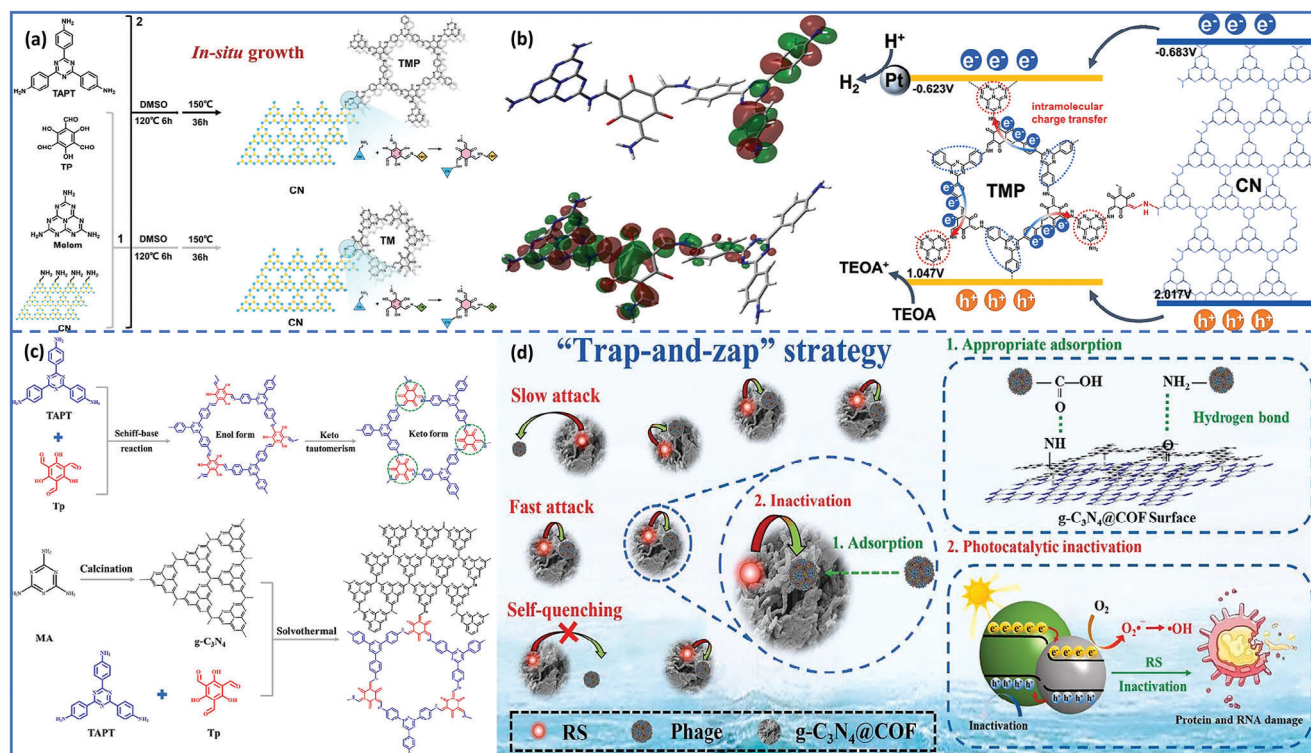


**Figure 5.** Constructing COFs-based metal-free heterojunction based on covalent bonding. a) Preparation diagram of CN/TMP and CN/TM. b) HOMO and LUMO of TMP COF's periodic unit via DFT calculation, and the possible intramolecular charge transfer mechanism of CN/TMP. Reproduced with permission.<sup>[39]</sup> Copyright 2022, Elsevier. c) The preparation and chemical structures of g-C<sub>3</sub>N<sub>4</sub>@COF, and the mechanism of virus appropriate adsorption and photocatalytic inactivation by g-C<sub>3</sub>N<sub>4</sub>@COF. Reproduced with permission.<sup>[27]</sup> Copyright 2022, Elsevier.

exhibits significantly improved charge delivery and a substantially reduced  $E_g$  compared to a COF-incorporated CN without TAPT participation (CN/TM). Moreover, PHE performance of CN/TMP revealed an enhancement of 5.6-fold and 11.6-fold compared to CN/TM and pristine CN, respectively. Similarly, Yu' group designed a triazine-based g-C<sub>3</sub>N<sub>4</sub>@COF heterojunction photocatalyst via in-situ growing COFs on g-C<sub>3</sub>N<sub>4</sub> with TP and TAPT (Figure 5c).<sup>[27]</sup> In contrast to g-C<sub>3</sub>N<sub>4</sub> alone, the g-C<sub>3</sub>N<sub>4</sub>@COF heterojunction exhibited superior exciton separation and quantum yield, along with a larger specific surface area and reduced negative charged surface. Consequently, g-C<sub>3</sub>N<sub>4</sub>@COF heterojunction is instrumental in virus adsorption and enhanced utilization efficiency of reactive species, leading to a 7.36-fold increase in virus inactivation compared to g-C<sub>3</sub>N<sub>4</sub>. Owing to the short half-life ( $10^{-6}$ – $10^{-9}$  s) of reactive species and their ready consumption by various constituents in water, the "trap-and-zap" strategy was put forward to improve affinity toward target degradation products and boost photocatalytic activity (Figure 5d).

### 2.3. Design Mechanisms

As discussed in above, apart from the staggered band alignment and intimate interface contact, efficient charge transfer is highly required in term of constructed a high-quality COFs-based metal-free heterojunctions. Two primary design mechanisms have been widely adopted to create COFs-based metal-free heterojunctions

with efficient charge transfer: enhance internal electric field (IEF) and built defects.

The most commonly used and effective measure to drive charge transfer is the enhancement of IEF. Generally, the intrinsic IEF for the highly symmetric single photocatalyst (e.g., COFs, g-C<sub>3</sub>N<sub>4</sub>) is negligible, which result to the ready recombination of photogenerated carriers. Breaking the symmetry via forming heterojunctions often adopt to alter the charge distribution and produce an induced interfacial IEF, and has been extensively discussed in many excellent papers.<sup>[60–62]</sup> The IEF in COFs-based metal-free heterojunction can adjust the driving force of charge dissociation and migration, and suppress carrier recombination. More importantly, the strong IEF could adjust charge migration direction to form a direct Z-scheme or S-scheme heterojunctions rather than a type II heterojunctions.<sup>[47]</sup> Dong et al.<sup>[63]</sup> developed 2D/2D S-scheme heterojunctions via the  $\pi$ – $\pi$  conjugation of  $\beta$ -ketoenamine-linked TpPa-1-COF with g-C<sub>3</sub>N<sub>4</sub> nanosheets. The disparity in the work functions of the two components led to a significant Fermi level gap, resulting in band edge bending of upward and downward. The spontaneous interfacial charge migration from g-C<sub>3</sub>N<sub>4</sub> to TpPa-1-COF at the  $\pi$ – $\pi$  conjugated interface generated a built-in electric field, which effectively driven directional charge transfer through S-scheme mechanism, thereby promoting charge migration and utilization (Figure 6a). The S-scheme heterostructure achieved the optimal PHE rate of 1153  $\mu\text{mol g}^{-1} \text{h}^{-1}$  under visible light irradiation. Coupling rGO and black phosphorene (BP) into TpPa-1 via a self-assembly strategy, Qin et al.<sup>[64]</sup> prepared a rGO/BP/TpPa-1

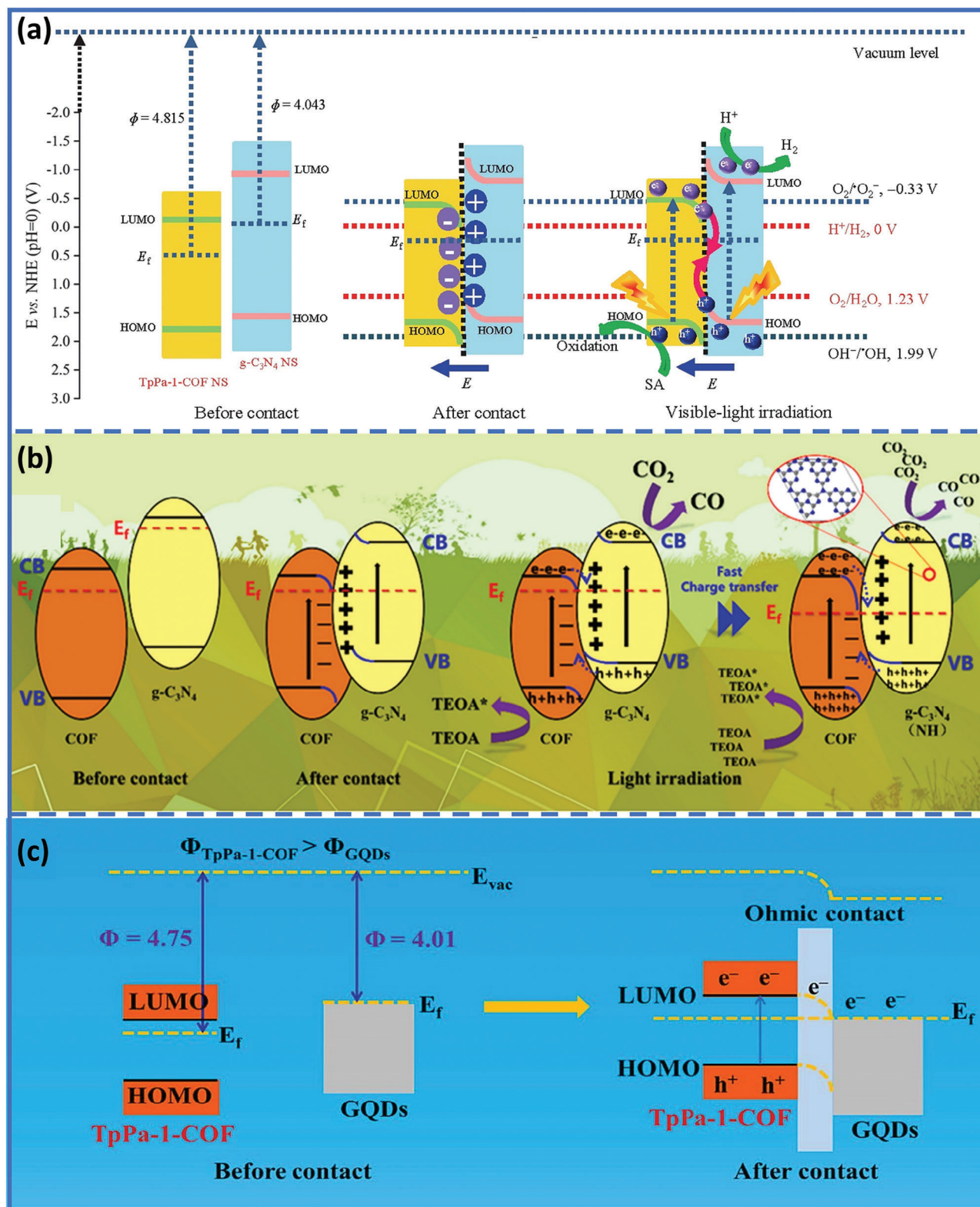


**Figure 6.** IEF and interfacial defects in constructing COFs-based metal-free heterojunctions. a) Charge migration mechanism of S-scheme TPCNS heterostructure before contact, after contact avoid light, and irradiated under visible-light. Reproduced with permission.<sup>[63]</sup> Copyright 2022, Elsevier. b) S-scheme charge transfer mechanism between Tp-Tta COF and  $g-C_3N_4$  (NH) with nitrogen vacancies. Reproduced with permission.<sup>[31]</sup> Copyright 2022, Elsevier. c) Possible structures of the energy band position and Fermi level of TpPa-1-COF and GQDs with Ohmic contact. Reproduced with permission.<sup>[65]</sup> Copyright 2023, Elsevier.

high-low heterostructure with a two-step photogenerated electron migration mechanism. Due to the difference in Fermi levels between BP and TpPa-1, an IEF can be established from BP to TpPa-1, resulting in the formation of a high-low heterojunction between TpPa-1 and BP. Consequently, electrons generated by TpPa-1 are transferred to BP, followed by migrate into rGO. Ultimately, rGO functioned as an electron acceptor for the reaction. The PHE rate of the ternary metal-free composite achieved  $18.09 \text{ mmol g}^{-1} \text{ h}^{-1}$ , exhibiting a remarkable 3.3-fold enhancement in contrast to that of pure TpPa-1.

Interfacial defects can also promote charge transfer, especially IEF is not strong enough to drive the dissociation and transfer of photogenerated charges.<sup>[47]</sup> Furthermore, abundant surface defects at the heterointerfaces would bring numerous quasi-continuous energy levels in the band gaps of the two components, leading to Ohmic contact with low electric resistance.<sup>[47]</sup> Coupling defective  $\text{C}_3\text{N}_4$  nanosheets ( $\text{C}_3\text{N}_4$  (NH)) with Tp-Tta COF with  $\pi$ - $\pi$  stacking interactions, Ye's group<sup>[31]</sup> reported a 2D/2D S-scheme heterojunction via a facile evaporation-induced self-assembly method. The appropriate nitrogen vacancies widened the Fermi level gap and created strong IEF, thereby accelerating the charge transfer at the VDW heterostructure interface via S-scheme pathway (Figure 6b). The resulting  $\text{C}_3\text{N}_4$  (NH)/COF S-scheme heterojunction revealed a stable and highly selective CO (90.4%) evolution rate of  $11.25 \mu\text{mol h}^{-1}$  upon visible-light illumination, which was significantly higher compared to the reference materials (45-fold for  $\text{C}_3\text{N}_4$  and 15-fold for  $\text{C}_3\text{N}_4$ /COF). Via deposited GQDs in the process of in situ synthesis of TpPa-1, Dong et al.<sup>[65]</sup> fabricated a GQDs modified  $\beta$ -ketoenamine-linked COF composite (GQDs/COF). The GQDs served as photosensitizer and electronic recipient to effectively broaden light absorption and collect photogenerated electrons to hold back following recombination of photogenerated carriers, while the Ohmic contact between GQDs, and COF promoted the fast transfer of photogenerated charges (Figure 6c). The obtained 0.44% GQDs/TpPa-1-COF presented PHE rate of  $487 \mu\text{mol g}^{-1} \text{ h}^{-1}$  upon visible-light illumination, improving 2.9 times in contrast to the pristine TpPa-1-COF.

With the rapid advancement of synthetic technologies, an increasing number of COFs-based metal-free heterojunctions have been reported. The representative examples include  $\text{g-C}_3\text{N}_4$ -COFs heterojunctions, carbon materials-COFs heterojunctions, polymer semiconductor-COFs heterojunctions, COFs-COFs heterojunctions and others. For ease of discussion, some COFs-based metal-free composites that do not explicitly indicate the formation of heterojunctions but facilitate interfacial charge transfer are also encompassed.

### 3. Typical COFs-Based Metal-Free Heterojunction Photocatalysts

#### 3.1. $\text{g-C}_3\text{N}_4$ -COFs Heterojunctions

As one of the most extensively studied metal-free semiconductor,  $\text{g-C}_3\text{N}_4$  possesses plentiful attractive merits such as raw materials cheap and readily accessible, preparation method facile, visible-light response, bandgap suitable and adjustable, stable physicochemical properties.<sup>[66,67]</sup> Since Professor Wang's ground-

breaking discovery of PHE capability of  $\text{g-C}_3\text{N}_4$  in 2009,<sup>[68]</sup> a plethora of functionalized materials and heterojunctions associated with  $\text{g-C}_3\text{N}_4$  have been developed for solar-to-chemical energy conversion.<sup>[69]</sup>  $\text{g-C}_3\text{N}_4$ -based COFs heterojunctions are the largest group of COFs-based metal-free heterojunctions, not only due to the above advantages of  $\text{g-C}_3\text{N}_4$ , but more importantly because of the merits of charge transport, easy construction, cost, and so on. Yan's group first reported the composite of COFs with  $\text{g-C}_3\text{N}_4$  via imine linkage for PHE.<sup>[70]</sup> Subsequently, they further modified CN nanosheet with trace COFs nanosheet via chemical imine bonding, which effectively passivated the surface termination of CN in the boundary region and built robust electronic coupling between the two components. This resulted in achieving the highest reported PHE rate for CN-based materials at that time ( $46.4 \text{ mmol g}^{-1} \text{ h}^{-1}$ , apparent quantum efficiency (AQE) of 31.8% at 425 nm).<sup>[71]</sup> Meanwhile, a series of COF/ $\text{g-C}_3\text{N}_4$  composites were synthesized for PHE,<sup>[47,72,73]</sup> pollutant degradation,<sup>[74–79]</sup>  $\text{CO}_2$  reduction,<sup>[80,81]</sup> etc.

As an all-organic semiconductor photocatalytic material,  $\text{g-C}_3\text{N}_4$  possesses pronounced conjugation effects like COFs, enabling facile construction of diverse heterojunctions with COFs through  $\pi$ - $\pi$  interactions, VDW forces, etc. Therefore, employing mild and straightforward methods such as self-assembly, grinding and solvothermal, can realize the synthesis of  $\text{g-C}_3\text{N}_4$ -COFs heterojunctions.<sup>[55,82]</sup> Via ultrasonic self-assembly with  $\pi$ - $\pi$  interactions (Figure 7a), Zeng' group<sup>[82]</sup> reported metal-free heterojunction (TpMa/CN) composed of pre-prepared CN and D-A conjugated TpMa COF, which used Tp and melamine (Ma) as blocks. The interface between TpMa and CN produced an inherent electric field that induced charge density redistribution, serving as the driving force for efficient charge carrier separation. The resulting TpMa/CN heterojunctions demonstrate significantly promoted photocatalytic activity toward tetracycline degradation and  $\text{H}_2\text{O}_2$  generation. Dispersing the powders (COF and  $\text{g-C}_3\text{N}_4$ ) in chloroform and sonicating for 10 min, followed by solvent evaporation at  $60^\circ\text{C}$  with stirring, COF/ $\text{g-C}_3\text{N}_4$  heterojunction was fabricated by Chou's group.<sup>[83]</sup> The COF rods, prepared through the assembly of benzothiadiazole and pyrene derivatives as building blocks, were integrated into 2D  $\text{g-C}_3\text{N}_4$  layer via intermolecular  $\pi$ - $\pi$  interactions. The resulted 30% COF/CN revealed a superior PHE rate of  $27\,540 \pm 805 \mu\text{mol g}^{-1} \text{ h}^{-1}$  with AQY of  $15.5 \pm 0.8\%$  (420 nm), exceeding most known  $\text{g-C}_3\text{N}_4$  and COFs-based photocatalysts. Via a simple solvothermal reaction, Professor Zhang's group<sup>[84]</sup> covalently grafted a Schiff-base COF with hydrazine units onto  $\text{g-C}_3\text{N}_4$ . They established a dynamic interface based on hydrogen bond interactions between TEOA and COF1, causing an evidently improved light harvest by COF1- $\text{g-C}_3\text{N}_4$  across the entire visible spectrum. The covalent link effectively accelerated photo-induced electron migration from COF1 to  $\text{g-C}_3\text{N}_4$ . The resultant metal-free COF1- $\text{g-C}_3\text{N}_4$  composite was utilized to directly convert  $\text{CO}_2$  in simulated flue gas into syngas, exhibiting catalytic activity of  $165.6 \mu\text{mol g}^{-1} \text{ h}^{-1}$ , surpassing the performance of previously reported metal-free catalysts under diluted  $\text{CO}_2$  conditions.

In situ preparation of  $\text{g-C}_3\text{N}_4$ -COFs heterojunctions is also achievable, which mainly synthesized COFs in situ on  $\text{g-C}_3\text{N}_4$ . Via in-situ condensation of 4,4'-Biphenyldicarboxaldehyde (BPC) and 4,4',4''-(1,3,5-triazine-2,4,6-triyl)trianiline (TTA) on the

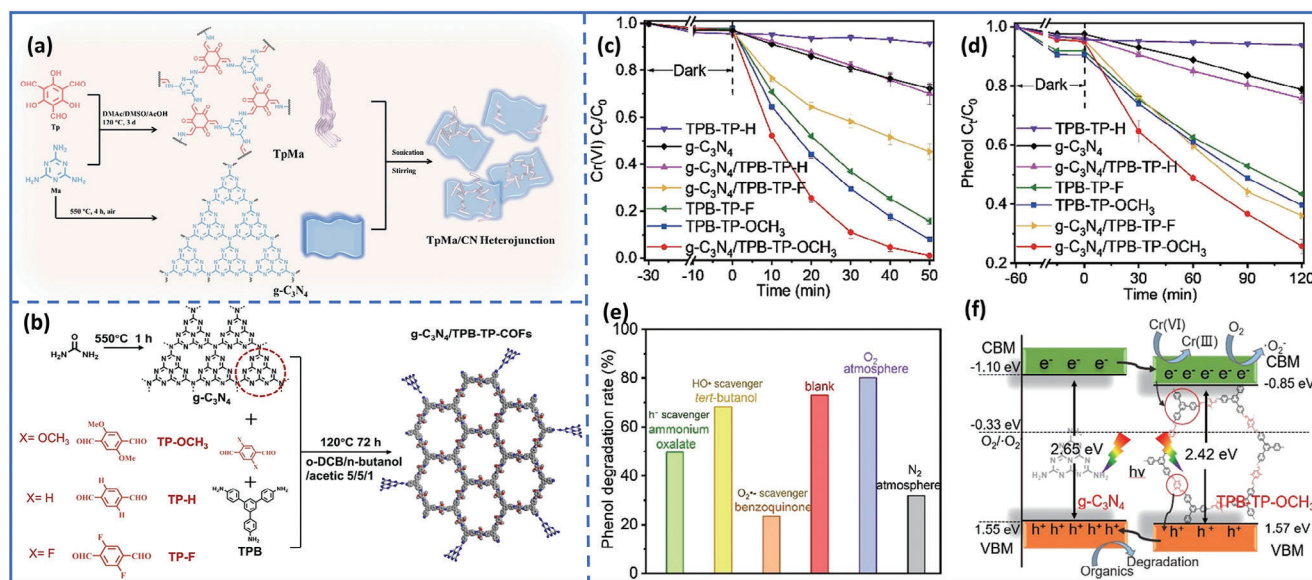


**Figure 7.** a) The synthesis process of TpMa/CN heterojunctions. Reproduced with permission.<sup>[82]</sup> Copyright 2022, Elsevier. b) Schematic synthetic route of g-C<sub>3</sub>N<sub>4</sub>/TPB-TP-COFs with diverse substituents. Photocatalytic Cr(VI) c) reduction and phenol degradation d) of g-C<sub>3</sub>N<sub>4</sub>, TPB-TP-COFs and g-C<sub>3</sub>N<sub>4</sub>/TPB-TP-COFs. e) Photocatalytic degradation of phenol over g-C<sub>3</sub>N<sub>4</sub>/TPB-TP-OCH<sub>3</sub> with different scavengers, under N<sub>2</sub> and O<sub>2</sub> atmosphere. f) Proposed mechanism of g-C<sub>3</sub>N<sub>4</sub>/TPB-TP-OCH<sub>3</sub> for removing phenol and Cr(VI). Reproduced with permission.<sup>[85]</sup> Copyright 2022, Springer.

surface of 2D CN, an all-organic 2D CN-COF catalyst was fabricated by Song et al.<sup>[57]</sup> for efficient photoreduction of CO<sub>2</sub>. The intense interface of VDW heterojunction induced a morphology transformation of COF-TD from isolated spherical particles to elliptical sheets within the 2D CN-COF. Additionally, the pronounced interface effect of VDW heterojunction resulted in a reduced bandgap, significantly expanding the visible light responsive region and suppressing charge carrier recombination. As a result, the evolution rate of CO over 2D CN-COF was 9.2 times and 3.3 times improvement than both 2D CN and COF-TD without any assistance from solvents or sacrificial agents. The substituents act crucial role in in-situ synthesis of g-C<sub>3</sub>N<sub>4</sub>-COFs heterojunctions.<sup>[85]</sup> TPB-TP-COFs, constructed from 1,3,5-tris(4-amino-phenyl)benzene (TPB) and terephthalaldehyde (TP) with various substituents (-H, -OH, -OCH<sub>3</sub>, -Br and -F groups, Figure 7b), were utilized by Ma et al.<sup>[85]</sup> for constructing g-C<sub>3</sub>N<sub>4</sub>/COFs, while bearing -OCH<sub>3</sub> groups can extremely promote both the photocatalytic Cr(VI) reduction and phenol oxidation (Figure 7c–e). The substituents can affect the dispersion of electron cloud of conduction band minimum (CBM), and the position of CBM in the TPB segment facilitated to the charge transfer between TPB-TP-OCH<sub>3</sub> and g-C<sub>3</sub>N<sub>4</sub> (Figure 7f). Employing a closed solvothermal method, Zhang's group<sup>[86]</sup> grown COF thin films with boronic ring on the surface of spongy g-C<sub>3</sub>N<sub>4</sub> using 4,4',4''-(1,3,5-triazine-2,4,6-triyl) trianiline and 4-formylphenylboronic acid as precursors. The formed S-scheme heterojunction significantly enhanced the electron accepting ability and propelled the generation of photogenerated carriers, thereby promoting surface catalytic reactions. The PHE rate achieved an impressive value of 7788.1 μmol h<sup>-1</sup> g<sup>-1</sup>, nearly seven times higher than that achieved by bare g-C<sub>3</sub>N<sub>4</sub>. Furthermore, this catalyst exhibited an AQE as high as 29.6%

### 3.2. Carbon Materials-COFs Heterojunctions

Typical semiconductors like COFs and g-C<sub>3</sub>N<sub>4</sub> possess the inherent high impedance and low conductivity characteristics, severely limiting charge transfer efficiency and weakening photocatalytic activity.<sup>[87]</sup> Inspired by the huge cost advantage, abundant earth natural resources, remarkable charge mobility and conductivity of carbon materials, carbon materials-COFs heterojunctions are expected to present further enhanced photocatalytic activity,<sup>[88]</sup> and becomes another major type of COFs-based metal-free heterojunctions. By incorporating GO into the preparation system of TpPa-1-COF, Yao et al.<sup>[89]</sup> realized one-pot reduction and functionalization of GO, while simultaneously covalently connecting it with COF. The covalent connection of rGO and TpPa-1-COF not only effectively combined these two types of 2D materials but also significantly enhanced the dissociation of photogenerated charges in COF and facilitated the migrate of electrons to rGO, thereby promoting PHE activity. In another research, via the in-situ assembly technique, Do et al.<sup>[90]</sup> anchored a ketoenamine-based COF onto rGO, achieving remarkable selectivity in the photoreduction of CO<sub>2</sub> to CO. The CO generation rate was ≈200 μmol g<sup>-1</sup> h<sup>-1</sup> and selectivity reaches 89%, which represented a 1.57- and 6.97-fold enhancement over the pristine COF and rGO, respectively. The covalent interaction between TpPa-1 and rGO not only conducive to create well-defined band edges with suitable potential, but also boosted effective separation and rapid migration of charge carriers to the material's surface for selectively reducing CO<sub>2</sub> to CO, an outcome corroborated by the <sup>13</sup>C labeling.

To promote exciton dissociation of COFs-based photocatalysts, highly conductive graphene quantum dots (GQDs) and carbon quantum dots (CQDs) are employed as charge acceptors or

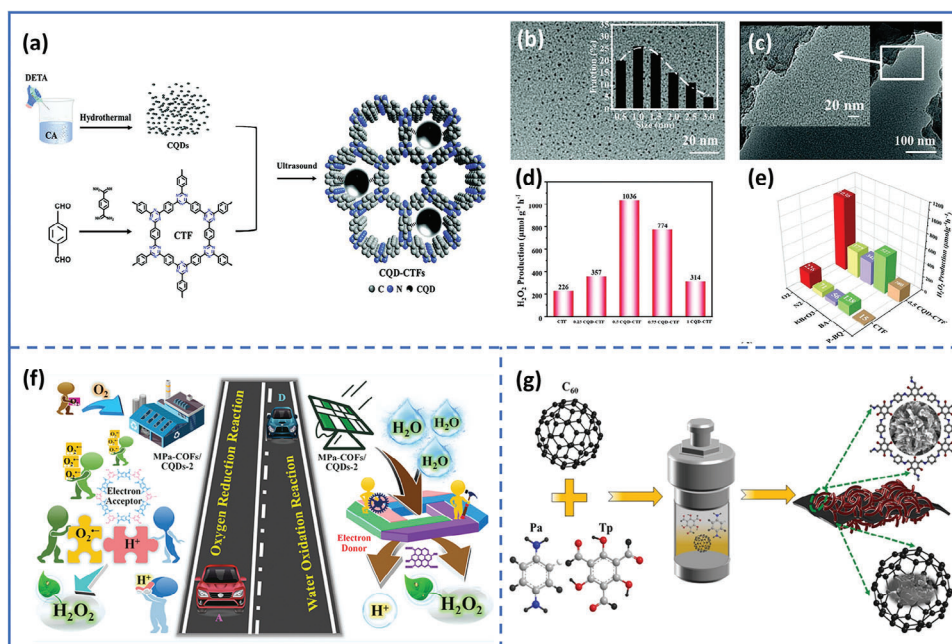


**Figure 8.** a) Scheme of the synthetic route of CQD-CTFs. Transmission electron microscopy image of CQDs b) and 0.5 CQD-CTF c). Photocatalytic H<sub>2</sub>O<sub>2</sub> production performance d) and capture experiments e) of CQD-CTFs. Reproduced with the permission of ref. [91] Copyright 2024, Wiley-VCH. f) Scheme of two-electron oxygen reduction reaction and the direct two-electron water oxidation reaction. g) Synthesis of C<sub>60</sub>/TpPa-X. Reproduced with permission.[94] Copyright 2023, Elsevier.

storage intermediary to drive the separation and transfer of excitons and charges.[65,91] Recently, Yang et al.[91] constructed a highly conductive confined CTF by utilizing CQDs as electron transport medium for efficient overall photocatalytic H<sub>2</sub>O<sub>2</sub> generation (Figure 8a). The uniform distribution and preferential localization of small-sized CQDs within the channels of CTF led to a remarkable 10-fold enhancement in conductivity compared to pure CTF (Figure 8b–e). The incorporation of CQDs enhanced the oxidation capacity and the affinity for H<sup>+</sup> owing to more negative zeta potential, which endowed a positive impact on both the water oxidation reaction and oxygen reduction reaction involved in H<sub>2</sub>O<sub>2</sub> generation. Remarkably, the optimized CQD-CTF composite revealed an impressive H<sub>2</sub>O<sub>2</sub> production rate of 1036 μmol g<sup>-1</sup> h<sup>-1</sup> upon visible-light illumination in pure water without assistant of sacrificial agent, surpassing that of alone CTF by a factor of 4.6. In another research, Lv et al.[92] decorated polyimide COFs with CQDs through one-pot hydrothermal approach. The introduction of CQDs not only reduced the impedance and suppressed carrier recombination but also broadened the visible-light harvest, as well as improved the hydrophilicity of polyimide COFs. The highest H<sub>2</sub>O<sub>2</sub> yield reached 540 μmol g<sup>-1</sup> within 1 h, which involved in both the step-by-step two-electron oxygen reduction reaction and the direct two-electron water oxidation reaction (Figure 8f).

Another common carbon-based material that integrates with COFs to form the heterojunction is fullerenes (C<sub>60</sub>). Since the electronic structure of C<sub>60</sub> is naturally concentrated on the surface of 30  $\pi$ -orbitals, the C<sub>60</sub>-COFs heterojunctions can achieve rapid photoinduced charge transfer. Encapsulating C<sub>60</sub> into the 1D channels of perylene-based COF via D-A interaction by Xu et al.,[93] the electrical conductivity of C<sub>60</sub>-COF significantly raised

from  $8.98 \times 10^{-8}$  to  $1.59 \times 10^{-5}$  S cm<sup>-1</sup>, meanwhile the carrier mobility increased from  $1.04 \times 10^{-3}$  to  $4.23 \times 10^{-2}$  cm<sup>2</sup> V<sup>-1</sup> s<sup>-1</sup> in contrast to single COF. In the work of He et al. in 2023,[94] a series of Z-scheme C<sub>60</sub>/TpPa heterojunction photocatalysts were first fabricated via in-situ solvothermal methods, where the TpPa-1 growth on C<sub>60</sub> using 1,3,5-triformylphloroglucinol (Tp) and paraphenylenediamine (Figure 8g). Owing to the formation of Z-scheme heterojunction, the photogenerated excitons were effectively separated, and the maximum CO formation rates of the heterojunction reached 48.16 and 90.25 μmol g<sup>-1</sup> h<sup>-1</sup> under pure and 10% CO<sub>2</sub> circumstance, respectively.

Most COFs are obtained with a powdered state via the solvothermal synthesis method, which leads to uneven and discontinuous charge/mass migration and diffusion processes, thereby limiting their applications.[95] Meanwhile, readily recovered photocatalysts in application systems, especially in aquatic environments with an easy-to-operate manner is highly desired. In contrast to the powder heterojunctions, heterojunction membranes exhibit greater potential for application in terms of stability, charge efficiency and recycling capabilities, ensuring the serviceability of COFs-based photocatalysts under various extreme conditions as pursued by researchers. Coupling hydrophilic COFs TpBD with carbon nanotube (CNT) interweaved porous membrane, Wang et al.[96] constructed COF/CNT composite membrane photocatalysts with eminent serviceability for dye degradation. The CNTs membranes served as large specific surface area substrates with excellent photothermal effect and electron transfer capacity, while the TpBD uniformly and firmly caught surface active groups on the membrane skeleton, thus accelerating the photocatalytic reaction and promoting mechanical strength of the composite membrane photocatalysts. The

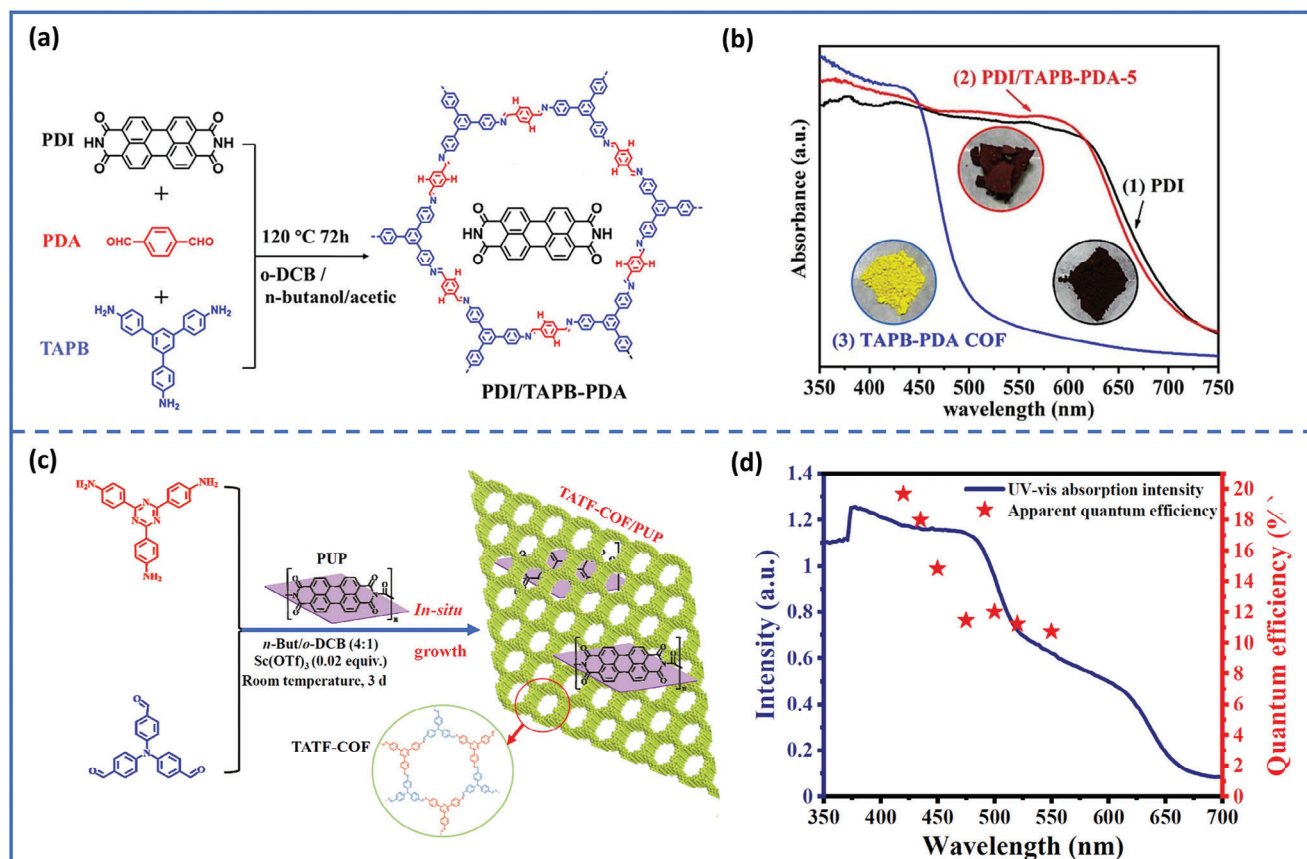


**Figure 9.** a) Schematic diagram of the synthesis of PDI/TAPB-PDA, b) UV-vis DRS of PDI, PDI/TAPB-PDA-5 and TAPB-PDA COF. Reproduced with permission.<sup>[98]</sup> Copyright 2023, Elsevier. c) Schematic of synthesizing the TATF-COF/PUP. d) Wavelength dependence of AQE.<sup>[99]</sup> Copyright 2023, Elsevier.

photocatalytic films achieved 708.2 mg g<sup>-1</sup> of total degradation capacity for mordant black 17, which only decreased 10.6% after recycling 7 times.

### 3.3. Polymer Semiconductor-COFs Heterojunctions

Other organic polymer semiconductors (e.g., PDI, perylene diimide urea polymer) can also form metal-free heterojunctions with COFs,<sup>[97–99]</sup> especially some polymers with excellent performances (e.g., suitable bandgap, low-cost, high light absorption intensity). Via solvothermal reaction of 1,3,5-tri(4-aminophenyl)benzene (TAPB) and terephthalaldehyde (PDA) under the presence of PDI, Professor Wang's group<sup>[98]</sup> successfully fabricated a PDI/COFs hybrid materials, taking advantage of their matching band structure (Figure 9a). The optimized PDI/TAPB-PDA-5 catalyst can photo-reduce Cr(VI) with the reaction rate 3.6 and 12.3 times, outperforming that of bare TAPB-PDA COF and PDI, respectively. The boosting photocatalytic activity ascribes to the significantly improved visible-light absorption capacity (Figure 9b) and promoted dissociation/migration of carrier. Through in situ growth 2D triazine-based imine linked COF (TATF-COF) on perylene diimide urea polymer (PUP) at room-temperature, Liang et al.<sup>[99]</sup> reported a conjugated COF/PUP metal-free S-scheme heterojunction with

accelerated carrier migration and prolonged carrier lifetimes (Figure 9c). The directional S-scheme charge migration (driven by the adjustable IEF) and the improved redox reaction rates of photogenerated carriers co-promoted the PHE performances. The optimized PHE rate reached 94.5 mmol h<sup>-1</sup> g<sup>-1</sup> (3.5 times that of single TATF-COF), and AQE achieved 19.7% at 420 nm (Figure 9d).

### 3.4. COFs-COFs Heterojunctions

Considering the compatibility issue between two photocatalysts, the fabrication of COFs-COFs heterojunctions is appealing. In contrast to other COFs-based metal-free heterojunction photocatalysts, achieving oriented creation of COFs-COFs heterojunctions through in situ synthesis is challenging due to the complex and ambiguous intermolecular interactions among different types of monomers as well as uncontrollable reaction processes.<sup>[100]</sup> Covalent organic nanosheets (CONs) also possess exceptional atomic precision assembly capability due to the remarkable designability of building blocks and diverse linkages. The CONs can be obtained through the exfoliation of COFs. Cai et al.<sup>[101]</sup> initially synthesized a PTO-COF featuring a well-ordered aldehyde groups within the channel. The PTO-COF was subsequently subjected to ball milling with Ma and Tp. The ball

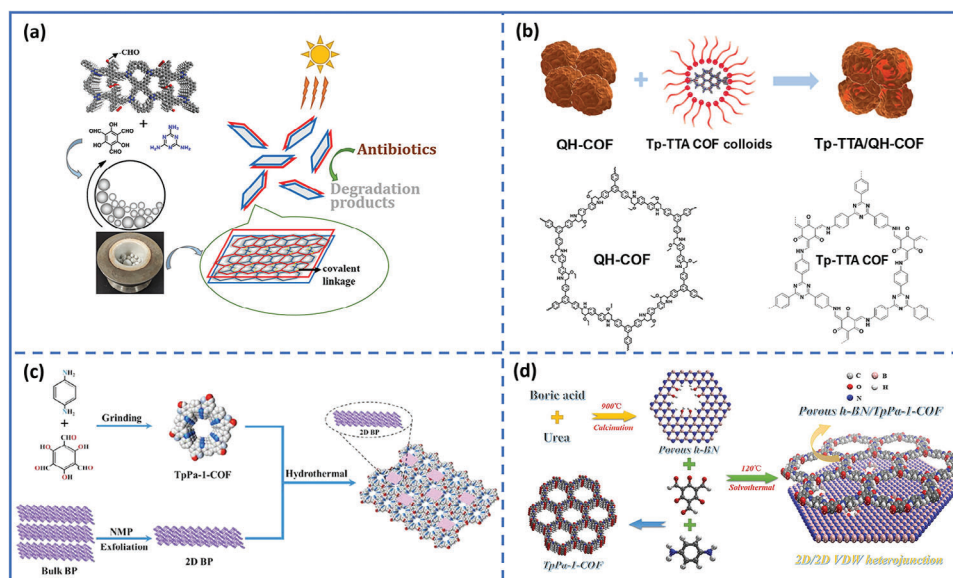


**Figure 10.** Synthesis route of 2D/2D TpMa/PTO CONs heterojunctions (a, reproduced with permission.<sup>[101]</sup> Copyright 2023, American Chemical Society), Tp-TTA/QH-COF heterojunction (b, Reproduced with permission.<sup>[29]</sup> Copyright 2022, Elsevier), BP/TpPa-1-COF p-n heterojunction (c, reproduced with permission.<sup>[102]</sup> Copyright 2022, Elsevier) and porous h-BN/TpPa-1-COF composites (d, reproduced with permission.<sup>[13]</sup> Copyright 2022, Springer).

milling processes exfoliated PTO-COF to produce PTO CONs and simultaneously synthesized TpMa-CONs, which covalently linked the aldehyde groups on PTO CONs through its amidogen, resulting in the in-situ synthesis of 2D/2D PTO/TpMa CONs hybrid materials (Figure 10a). The LUMO of TpMa-CONs and the HOMO of PTO-CON covalently linked to form a Z-scheme heterojunction, which promoted visible light photodegradation activity in contrast to individual 2D TpMa-CON and TpMa-COF.

In contrast to in-situ fabrication COFs-COFs hybrid structure, deposition and assembly with controllable ratio and location of individual COFs via intermolecular interactions also welcomed. Depositing nano Tp-TTA COF colloids on tetrahydroquinoline-linked QH-COF, Yang et al.<sup>[29]</sup> constructed a COFs-COFs heterojunctions with enhancing conductivity and photocurrent response, as well as boosting exciton dissociation effect in contrast to single COFs (Figure 10b). The intimate contact between the two COFs formed n-n heterojunction, which promoted the charge separation. The resultant Tp-TTA/QH COF-COF heterojunction also possessed a high crystallinity and BET surface areas, and superior visible light response, which led more exceedingly photocatalytic activity in the 3,5,3',5'-tetramethyl-benzidine and benzyl alcohol oxidation. Through a liquid-phase assembly method, Xu et al.<sup>[38]</sup> constructed a 2D-2D P-COF-1/CTF heterojunction of triphenylphosphine-based COF (P-COF-1)/covalent triazine framework (CTF), demonstrating remarkable activity and stability for PHE. The synergistic effect between these two COFs formed a type II heterojunction system through intermolecular  $\pi$ - $\pi$  interactions, leading to extended the visible light harvest and notably improved the dissociation efficiency of photogenerated exciton. The PHE rate of 5% P-COF-1/CTF heterojunction reached  $14\ 100\ \mu\text{mol h}^{-1}\text{ g}^{-1}$ , which is  $\approx 2.5$ – $2.6$  times higher than that of simple CTF and their mechanical mixture (5% P-COF-1 + CTF).

### 3.5. Other Metal-Free Semiconductor-COFs Heterojunctions

The insufficient interfacial contact between the two components in 0D/2D and 1D/2D heterojunctions often hampers charge transfer, as the produced charges undergo a lengthy journey to reach the surface, resulting in significant recombination that ultimately decrease photocatalytic activity.<sup>[63]</sup> As discussed in the section of “Interaction of heterointerfaces”, 2D/2D COFs-based metal-free heterojunctions possess more advantages in contact area and shorter transfer distance. Apart from  $\text{g-C}_3\text{N}_4$ , GO, some other metal-free semiconductor, especially some rising 2D material are also welcomed to fabricated COFs-based metal-free heterojunctions.

BP, an emerging 2D material with superior merits of tunable bandgap, optical properties and electronic behavior, is a promising alternative to fabricate metal-free heterojunction photocatalysts.<sup>[102]</sup> As a typical p-type semiconductor, BP can form a p-n junction with n-type TpPa-1-COF, which can accelerate detachment and transport of charges due to the establishment of IEF at the heterojunction contact interface. By a facile solvothermal method, Professor Wu's group<sup>[102]</sup> fabricated a metal-free 2D-2D BP/TpPa-1-COF p-n heterojunction (Figure 10c). Owing to effective migration of photogenerated excitons and carriers at the dense contact of 2D-2D heterojunction interface, the obtained highest PHE rate reached  $456.7\ \mu\text{mol g}^{-1}\text{ h}^{-1}$  without loading precious metal, which is 13-fold and 24-fold increase in contrast to that of pure TpPa-1-COF and 2D BP flakes, respectively.

Hexagonal boron nitride (h-BN), also known as white graphene due to its honeycomb 2D structure, is composed of lightweight elements with distinctive physicochemical characters. After fully investigating the virtues of defect h-BN and VDW heterojunctions, Yang et al.<sup>[13]</sup> proved that the integration of 2D COFs with defect-engineered h-BN would present

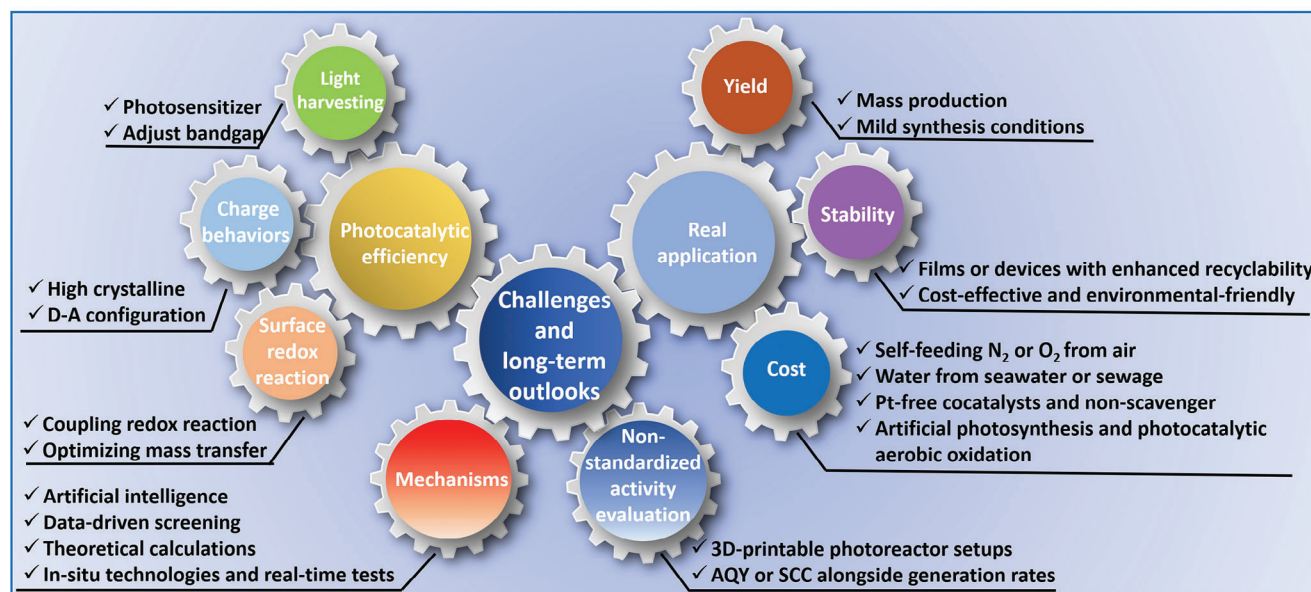


**Figure 11.** Challenges and long-term outlooks of COFs-based metal-free heterojunction photocatalysts.

promising prospects for fabricating non-metallic COFs-based heterojunctions. Utilizing an effortless calcination solvothermal approach, the research group successfully synthesized a novel metal-free 2D/2D VDW heterojunction by combining a 2D ketoenamine-linked defective COF (TpPa-1-COF) with porous h-BN (Figure 10d). The h-BN supplied additional reactive sites, and led to a structural transformation in TpPa-1-COF, which elevated the CB position of TpPa-1-COF and enlarged the CB gap between the two components, thus effectively suppressing electron back-flow. The VDW heterojunction facilitated a larger contact area and compact electronic coupling at the interface between TpPa-1-COF and defective h-BN, thereby enhancing charges separation. The activity of h-BN/TpPa-1-COF metal-free VDW heterojunction is extremely boosted with a record-breaking PHE rate of  $3.15 \text{ mmol g}^{-1} \text{ h}^{-1}$  in metal-free photocatalysts without participation of co-catalysts.

## 4. Conclusion, Challenges and Long-Term Outlooks

With the continuous progress in technology, science, and the exhaustion of fossil energy, COFs-based metal-free heterojunctions reveal great potential in solar-to-chemical energy conversion owing to their merits of environmentally friendly and cost-competitive, as well as adjustable structure. In this review, we systematically summarized the advances in COFs-based metal-free heterojunctions for the first time from heterojunction types, heterointerfaces interactions, and primary design mechanisms. Then, several typical COFs-based metal-free heterojunction photocatalysts are introduced. Although the remarkable advancements have been achieved in COFs-based metal-free heterojunctions for solar-to-chemical energy conversion (Table 1), numerous challenges persist, necessitating further time and effort. Herein, we present the challenges and long-term prospects of

COFs-based metal-free heterojunction photocatalysts from four distinct perspectives (Figure 11).

### 4.1. Photocatalytic Efficiency

The high photocatalytic efficiency has always been pursued, relying on light harvesting (optoelectronic properties, well-matched band structure), photogenerated charge behaviors (e.g., excitation, relaxation, migration and recombination) and surface redox reaction (adsorption, catalytic sites, mass transfer).<sup>[1,7]</sup>

In aspects of light absorption, various strategies, such as functional group modification, doping, constructing D-A heterojunctions and redox molecular junctions, have been reported to adjust bandgap and enhance the optoelectronic properties of COFs-based metal-free heterojunctions.<sup>[34,103,104]</sup> Additionally, incorporating photosensitizer units into COFs is also an effective approach to improve light absorption.<sup>[65]</sup> Recently, the research group of Professor Lan rationally designed a series of three-motif molecular junction type COFs, which formed dual photosensitizers coupled redox molecular junctions COFs for photocatalytic aerobic oxidation reactions.<sup>[33]</sup> Due to the strong light harvest capacity of dual photosensitizer units and the integrated redox features, the photocatalytic benzylamine conversion efficiency within 2.5 h reached 99.9% and selectivity nearly 100%.

In terms of adjusting charge behaviors, the high exciton binding energy in polymer semiconductors (often  $>300 \text{ meV}$ ) poses challenges for efficient dissociation of photogenerated excitons and generation of carriers (energized  $e^-$  and  $h^+$ ) to participate in subsequent surface reactions, thereby significantly limiting photocatalytic performance.<sup>[105]</sup> Strategies such as enhancing crystalline and constructing D-A structures are commonly employed to enhance the IEF of COFs and modulate charge behaviors. Meanwhile, a balance between charge carrier lifetimes and catalysis timescales should be consideration.

**Table 1.** Comparison of COFs-based metal-free heterojunction photocatalysts according to different Applications.

Catalyst	Designing strategy	Building blocks of COFs	Heterojunction type, charge transfer mechanism and interaction	Application, Performances, improvement times	Refs.
<i>h</i> -BN/TpPa-1-COF	Calcination solvothermal approach	1,3,5-triformylphloroglucinol (Tp) paraphenylenediamine (Pa-1)	VDW heterojunction, Larger contact area and intimate electronic coupling	PHE rate is 3.15 mmol g <sup>-1</sup> h <sup>-1</sup> without participation of co-catalysts, 67 times than pristine TpPa-1-COF	[13]
P-COF-1/CTF	Liquid-phase assembly method	Tris (4-formylphenyl) phosphine 1,4-benzenedimethanol terephthalamide dihydrochloride	Type II heterojunction via intermolecular $\pi$ - $\pi$ interactions	PHE rate is 14 100 $\mu$ mol h <sup>-1</sup> g <sup>-1</sup> , 2.5–2.6 times higher than pure CTF and their mechanical mixture	[38]
CN/TMP	One-pot solvothermal method to in-situ grow a nitrogen-rich COF TMP onto CN	Melem 1,3,5-triformylphloroglucinol (TP) 2,4,6-tris(4-aminophenyl)-1,3,5-triazine (TAPT)	Cocoon-like morphology ICT influence within the TMP Raised charge delivery and lowered band gap energy	PHE rate is 102.88 $\mu$ mol h <sup>-1</sup> , 5.6 and 11.6 times than CN/TM and CN	[39]
PeCOF-1/PCN	Assembly via $\pi$ - $\pi$ interaction	Tri-(4-formylphenyl)phosphine (TFP) p-phenylenediamine	Type-II heterojunction with $\pi$ - $\pi^*$ and n- $\pi^*$ electrons transition	PHE rate is 1 105 $\mu$ mol h <sup>-1</sup> g <sup>-1</sup> , 12 times than pure PCN	[47]
COF/CN	Ultrasonic method	1,3,5-triformylphloroglucinol (TP) pphenylenediamine (PDA)	2D/2D VDW heterojunctions	PHE rate is 449.64 $\mu$ mol h <sup>-1</sup> , 5 times than pure CN	[56]
rGO/BP/TpPa-1	Self-assembly strategy	1,3,5-triformylphloroglucinol (Tp) Paraphenylenediamine (Pa)	High-low heterostructure, Photogenerated electrons generated by TpPa-1 are transferred to BP, followed by transfer into rGO	PHE rate is 18.09 mmol g <sup>-1</sup> h <sup>-1</sup> , 3.3-fold enhancement compared to that of pure TpPa-1	[64]
GQDs/TpPa-1-COF	Deposited GQDs in the process of in-situ synthesis of TpPa-1	p-toluene sulphonic acid (PTSA) p-phenylenediamine (Pa-1) 1,3,5-triformylphloroglucinol (Tp)	Ohmic contact effect between the TpPa-1-COF and GQDs	PHE rate is 487 $\mu$ mol g <sup>-1</sup> h <sup>-1</sup> , 2.9 times compared to bare TpPa-1-COF	[65]
CN-COF	Co-condensation of TP, TTA and g-C <sub>3</sub> N <sub>4</sub> by a solvothermal reaction	4,4',4''-(1,3,5-triazine-2,4,6-triyl)trianiline (TTA) 1,3,5-triformylphloroglucinol (TP)	Modify g-C <sub>3</sub> N <sub>4</sub> with COFs through imine bonding	PHE rate is 10.1 mmol g <sup>-1</sup> h <sup>-1</sup> AQE of 20.7% at 425 nm	[70]
CNS-600-COF	Thermal exfoliated CN integrated with a small number of imine-linked COFs	4,4',4''-(1,3,5-triazine-2,4,6-triyl)trianiline (TTA) 1,3,5-triformylphloroglucinol (TP)	Modify CNS with COF through imine bonding, strong electron coupling leads to more efficient charge separation	PHE rate is 46.4 mmol g <sup>-1</sup> h <sup>-1</sup> AQE is 31.8% at 425 nm	[71]
COF-CN	In situ reaction of Tp and BD in stripped g-C <sub>3</sub> N <sub>4</sub> suspension	2,4,6-triformylphloroglucinol (Tp) Benzidine (BD)	Type II heterojunction Large and intimate interface contact	PHE rate is 12.8 mmol g <sup>-1</sup> h <sup>-1</sup> , 62 and 284 times than COF and g-C <sub>3</sub> N <sub>4</sub> AQE is 15.09% at 500 nm	[72]

(Continued)

**Table 1.** (Continued)

Catalyst	Designing strategy	Building blocks of COFs	Heterojunction type, charge transfer mechanism and Interaction	Application, Performances, Improvement times	Refs.
TBTA/g-C <sub>3</sub> N <sub>4</sub>	In-situ condensation of TP and BTDA on g-C <sub>3</sub> N <sub>4</sub>	2,4,6-triformylphloroglucinol (TP) 4,4'-(benzo-1,2,5-thiadiazole-4,7-diyl)dianiline (BTDA)	Intermolecular $\pi$ - $\pi$ interactions forming hybrids. D-A framework TBTA serves as a photosensitizer	PHE rate is 11.73 mmol g <sup>-1</sup> h <sup>-1</sup> without a noble metal, 26.04 mmol g <sup>-1</sup> h <sup>-1</sup> with Pt as a co-catalyst	[73]
COF/CN	Solvent evaporation self-assembly	Benzothiadiazole (BT) Pyrene (Py)	Type-II heterojunction, Intermolecular $\pi$ - $\pi$ interactions	PHE rate is 27 540 $\pm$ 805 $\mu$ mol g <sup>-1</sup> h <sup>-1</sup> , AQY is 15.5 $\pm$ 0.8%	[83]
CN/COF	Solothermal method grown COF thin films with boric ring on the surface of spongy g-C <sub>3</sub> N <sub>4</sub>	4,4'-4''-(1,3,5-triazine-2,4,6-triyl) trianiline 4-formylphenylboronic acid	S-scheme heterojunction	PHE rate is 7788.10 $\mu$ mol h <sup>-1</sup> g <sup>-1</sup> , 7 times than g-C <sub>3</sub> N <sub>4</sub> , AQE is 29.6%	[86]
rGO-TpPa-1-COF	Covalent connection of rGO and TpPa-1-COF	1,3,5-triformylphloroglucinol (Tp) p-phenylenediamine (PPD)	Covalent connection between the rGO and TpPa-1-COF	PHE rate is 11.98 mmol g <sup>-1</sup> h <sup>-1</sup> , 4.85 and 2.50 times than pure TpPa-1-COF and 5%rGO/TpPa-1-COF	[89]
TATF-COF/PUP	In situ coupling of the 2D triazine-based imine-linked COF (denoted as TATF-COF) with PUP	2,4,6-tris(4-aminophenyl)triazine (TA) tris(4-formylphenyl)amine (TF)	Organic PUP/COFs S-scheme heterojunction	PHE rate is 94.5 mmol h <sup>-1</sup> g <sup>-1</sup> , 3.5 times than pure TATF-COF, AQE is 19.7% at 420 nm	[99]
BP/TPa-1-COF	Solothermal approach	p-phenylenediamine (Pa-1) 1,3,5-triformylphloroglucinol (Tp)	Metal-free 2D-2D BP/TpPa-1-COF p-n heterojunction	PHE rate is 456.7 mmol h <sup>-1</sup> g <sup>-1</sup> , 13 times than pristine TpPa-1-COF and 24 times than 2D BP flakes	[102]
CNTD	Solothermal method	2,6-diaminoanthraquinone (DAAQ) 1,3,5-triformylphloroglucinol (TFP)	Graphitic CN (GCN)/anthraquinone-based COF (TD-COF) VDW heterojunction	Degradation of phenolic wastewater 99.4% within 12 min, 204.2 and 26.8 times than GCN and TD-COF	[75]
UCN@COF	Thermal treatment to form hierarchical g-C <sub>3</sub> N <sub>4</sub> @COF hybrids	1,3,5-triformylphloroglucinol p-phenylenediamine	Aggregated COFs crystals anchored on the irregular g-C <sub>3</sub> N <sub>4</sub> surface to form 3D structure	Orange II removal (100% within 45 min) compared to pristine g-C <sub>3</sub> N <sub>4</sub> (10%) and COF (5%)	[76]
CNNS/TPA-COF	TPA-COF was grown on the surface of the CNNS to obtain a COF modified CNNS	1,3,5-triformylphloroglucinol p-phenylenediamine	2D/2D CNNS/TPACOF heterojunction	CNNS/TPA-COF-2 nearly 100% photodegraded RHB within 40 min, CNNS and TPACOF for RHB are 65% and 63%	[77]

(Continued)

**Table 1.** (Continued)

Catalyst	Designing strategy	Building blocks of COFs	Heterojunction type, charge transfer mechanism and interaction	Application, Performances, improvement times	Refs.
COF-CNNS	In-situ synthesis of metal-free COF-CNNS hybrid	terephthalaldehyde (PD) 1,3,5-tri(4-aminophenyl)benzene (TPB)	Type II heterojunction IEF promotes directional charge transfer	Remove > 99% of Cr(VI) in 30 min $k_{app}$ is 0.141 min <sup>-1</sup> , 32 and 5 times than CNNS and TPBPD-COF	[79]
TpMa/CN	TpMa could be introduced into g-C <sub>3</sub> N <sub>4</sub> via self-assembly due to $\pi$ - $\pi$ interactions	1,3,5-triformylphloroglucinol aldehyde Ma	Type-II heterojunction IEF is formed at the interface of composite	k of TC degradation is 0.02620, 2.3 and 4.3 times than TpMa and CN, H <sub>2</sub> O <sub>2</sub> production is 880.494 $\mu$ M h <sup>-1</sup> , 49 times than CN	[82]
g-C <sub>3</sub> N <sub>4</sub> /TPB-TP-OCH <sub>3</sub>	COFs with different electronegative substituents	1,3,5-tris(4-amino-phenyl)benzene (TPB) Dimethoxyterephthalaldehyde (TP-OCH <sub>3</sub> )	Type-II heterojunction, Electronic effects of substituents	Photocatalytic Cr(VI) reduction (120 min, 70%+) and phenol degradation (50 min, 100%)	[85]
COF/CNT membrane	In-situ synthesis of COF on carbon nanotube interweaved porous membrane	2,4,6-triformylphloroglucinol (Tp) Benzidine (BD)	CNT membranes COF synergism	MB17 degradation capacity is 708.2 mg g <sup>-1</sup>	[96]
PDI/TAPB-PD	In-situ synthesis of COF on PDI	1,3,5-tri(4-aminophenyl)benzene (TAPB) Terephthalaldehyde (PDA)	Type II heterojunction based on COF and PDI matching band structure	Cr(VI) reduction, k is 0.047 min <sup>-1</sup> , 12.3 and 3.6 times than PDI and TAPB-PDA COF	[98]
PTO/TpMa CONS	Ball milling processes	1,3,6,8-tetrakis(p-formylphenyl)-pyrene (TFPPy) 2,4,6-trimethyl-1,3,5-triazine (TMT) 1,3,5-triformylphloroglucinol (Tp) Ma	Z-scheme heterojunction	Degradation rate is 98.4% Rate constant is 1.04 $\times 10^{-3}$ s <sup>-1</sup> , 2.22 times that of PTO-CON and 1.94 times that of TpMa-CON	[101]
CQD-CTF	CTF with the assistance of CQDs as the electron transport mediums	1,4-phthalaldehyde terephthalamidine dihydrochloride	Confined CTF with CQDs as electron transport medium	H <sub>2</sub> O <sub>2</sub> generation rate is 1036 $\mu$ mol g <sup>-1</sup> h <sup>-1</sup> , 4.6 times than pristine CTF	[91]
MPa-COFs/CQDs-2	Decorated polyimide COFs with CQDs via one-pot hydrothermal approach	Ma, pyromellitic anhydride, 1,4,5,8-naphthalenetetracarboxylic dianhydride	Electron donor-acceptor interaction between polyimide COFs and CQDs	The highest H <sub>2</sub> O <sub>2</sub> generation rate is 540 $\mu$ mol g <sup>-1</sup> within 60 min	[92]
COF@CDs	Binary system with a D-A type COF and CDs as both the electron extractant and storage media	4,4',4''-(1,3,5-triazine-2,4,6-yl) trianiline (TTA) 1,3,5-triformylphloroglucinol (Tp)	Intramolecular charge transfer between D-A semiconductors and polymers with $\text{=C=O-H-N}$ = hydrogen-bonding groups	Photocatalytic sterilization efficiency over 95% in 1 h, decrease in the survival rate by 8.3 times compared of COF	[59]

(Continued)

**Table 1.** (Continued)

Catalyst	Designing strategy	Building blocks of COFs	Heterojunction type, charge transfer mechanism and interaction	Application, Performances, improvement times	Refs.
$g-C_3N_4@COF$	In-situ synthesis of COF on $g-C_3N_4$	2,4,6-trihydroxybenzene-1,3,5-tricarbaldehyde 2,4,6-tris(4-aminophenyl)-1,3,5-triazine	2D/2D type-II heterojunction	Photocatalytic antibacterial, removal rate constant is $0.2502 \text{ min}^{-1}$ , 7.36 and 2.31 times than $g-C_3N_4$ and COF	[27]
Tp-TTA/QH	Depositing nano Tp-TTA COF colloids on tetrahydroquinoline-linked QH-COF	1,3,5-triformylphloroglucinol (Tp) 4,4',4''-(1,3,5-triazine-2,4,6-tryl)trianiline (TTA) 1,3,5-tris(p-formylphenyl)benzene, benzidine	n-n heterojunction High crystallinity and BET surface areas	Selective oxidation of benzyl alcohol, the turnover frequency is $1.25 \text{ mmol g}^{-1} \text{ h}^{-1}$ , 2.2 and 3.9 times than QH-COF and Tp-TTA COF	[29]
PY-BT COF	Three-motif molecular junction	BT PY	Redox heterojunction Synergistic effect of dual photosensitizer coupled redox molecular junction COFs.	Photocatalytic benzylamine oxidation, Conversion efficiency of 99.9% in 2.5 h,	[33]
$C_3N_4$ (NH)/COF	Evaporation induced self-assembly method	4,4',4''-(1,3,5-triazine-2,4,6-tryl) trianiline (TTA) 1,3,5-triformylphloroglucinol (Tp)	S-scheme heterojunction, Appropriate nitrogen vacancies and strong IEF due to $\pi-\pi$ stacking interactions	$CO_2$ reduction, CO selective is 90.4%, generation rate is $11.25 \mu\text{mol h}^{-1}$ , 45 times and 15 times than $g-C_3N_4$ and $g-C_3N_4/COF$	[31]
$COF1-g-C_3N_4$	Solvothermal reaction	2,4,6-tri(4-vinylbenzoyl)-s-triazine (TVBT) and N-amino-4-hydrazino-1,8-naphthalimide (NAHN)	Covalently grafting COF1 with $g-C_3N_4$ accelerated photo-induced electron transfer	Directly converts $CO_2$ in the simulated flue gas to syngas with the catalytic activity of $165.6 \mu\text{mol g}^{-1} \text{ h}^{-1}$	[84]
$rGO15@TpPa-1$	In situ growth of TpPa-1 on rGO	1,3,5-triformylphloroglucinol (Tp) p-phenylenediamine (Pa)	Covalent interactions improved charge separation and migration to surface for selective reduction of $CO_2$ to CO	Yielded the CO at a rate up to $\approx 200 \mu\text{mol g}^{-1} \text{ h}^{-1}$ and with a selectivity of 89%, 1.57 and 6.97 times higher to bare COF and rGO.	[90]
PRGO/TP-COF	Electrostatic self-assembly method	2,4,6-tris(4-formylphenyl)-1,3,5-triazine (TFPT) 1,4-phenylenediacetonitrile (PDAN)	S-scheme heterojunction $\pi-\pi$ interaction	$CO_2$ reduction, CO yields is 48.81, 1.72 times than pure TP-COF and 4.93 times than pure PRGO	[32]
COF: $g-C_3N_4$	In-situ synthesized COF on the template of $g-C_3N_4$	Cyanuric chloride 4,4'-bipyridine precursors	Type II heterojunction Delocalized $\pi$ -conjugated systems	$CO_2$ reduction, CO yield of $7.56 \mu\text{mol g}^{-1} \text{ h}^{-1}$	[81]

(Continued)

**Table 1.** (Continued)

Catalyst	Designing strategy	Building blocks of COFs	Heterojunction type, charge transfer mechanism and interaction	Application, Performances, improvement times	Refs.
2D CN-COF	Interface VDW force interaction between 2D CN and COF-TD	4,4'-Biphenyldicarboxaldehyde (BPC) 4,4',4''-(1,3,5-triazine-2,4,6-triyl)trianiline (TTA)	VDW heterojunction $\pi$ - $\pi$ interaction	CO <sub>2</sub> reduction, afford CO and CH <sub>4</sub> evolution rate of 7.08 and 2.37 $\mu\text{mol g}^{-1} \text{h}^{-1}$ , the evolution rate of CO is 9.2 and 3.3 times than 2D CN and COF-TD	[57]
C <sub>60</sub> /TpPa	In-situ solvothermal method	1,3,5-triformylphloroglucinol Paraphenylenediamine	Z-scheme heterojunction Electrostatic attraction	CO <sub>2</sub> reduction, CO formation rates is 48.16 and 90.25 $\mu\text{mol g}^{-1} \text{h}^{-1}$ under pure and 10% CO <sub>2</sub> , 3.4 times than TpPa-1 at 10% CO <sub>2</sub>	[94]

When considering surface redox reactions, the primary focus lies on active sites for adsorption and catalysis. The porous structure of COFs not only facilitates the loading of co-catalysts as additional catalytic sites but also enables the adsorption of various substrates, such as PMS for synergistic photodegradation of pollutants, oxygen, nitrogen, or alcohols for hydrogen peroxide production, nitrogen fixation, and high-value chemical synthesis.<sup>[3]</sup> Constructing COFs-based metal-free heterojunctions offers the potential to create more active sites while exploring additional functional units to optimize surface redox reactions (e.g., introducing diacetylene and Bpy into COFs to enhance H<sub>2</sub>O<sub>2</sub> generation).<sup>[105]</sup> Furthermore, optimizing mass transfer can aid in maximizing substrate utilization in these reactions. Hu et al. designed a gas-liquid-solid interface system to enhance O<sub>2</sub> solubility and diffusion rate significantly, thereby promoting oxygen mass transfer and facilitating H<sub>2</sub>O<sub>2</sub> generation.<sup>[106]</sup> Additionally, coupling oxidation and reduction reactions simultaneously allows for the fully separate photogenerated excitons and maximization of total solar energy utilization efficiency. The group of Professor Lan coupled a H<sub>2</sub>O<sub>2</sub> production system and value-added biomass furoic acid production, and the solar chemical conversion (SCC) reached 0.62%.<sup>[107]</sup>

## 4.2. Yield, Stability and Cost

Although there has been growing body of COFs-based metal-free heterojunctions, the majority of COFs preparation still remains at the laboratory level with production limited to milligrams level, hindering large-scale preparation and practical applications. Hence, it is imperative to develop synthesis strategies for COFs that facilitate mass production to meet industrial demands. Zhang et al. successfully synthesized neutral and ionic ethylene COFs through a cost-effective melt polymerization method,<sup>[108]</sup> achieving high yields in kilograms at an extremely low cost (<50 USD kg<sup>-1</sup>). This innovative synthesis strategy paves the possibilities for large-scale industrial generation of ionic COFs. Furthermore, although the solvothermal reaction is the most widely used method, its harsh synthesis conditions, e.g., long reaction time, high temperature or pressure, make it unsuitable for large-scale application. Consequently, there is a need for low-cost yet effective synthesis strategies with mild reaction conditions such as mechanical and ultrasound method to synthesize COFs-based metal-free heterostructures with boosted photocatalytic activity.

Although COFs are associated with relatively stable covalent bonds that can partially fulfill the requirements of photocatalytic reactions (e.g., PHE and photocatalytic CO<sub>2</sub> reduction), their photochemical stability should be taken into consideration in some photocatalytic reactions (e.g., persulfate oxidation and hydrogen peroxide production) involving strong oxidants, especially at high concentrations. Therefore, it is reasonable to construct heterostructure photocatalytic films<sup>[17]</sup> or devices based on COFs, and utilize the metal-free part to enhance recyclability.

The expensive nature of COFs linkers and harsh synthesis conditions have prompted researchers to explore new approaches that are both cost-effective and environmental-friendly. Moreover, strategies such as self-feeding N<sub>2</sub> or O<sub>2</sub> from air, water from seawater or sewage, Pt-free cocatalysts for HER, as well as the

use of non-scavenger systems or sustainable sacrificial reagents would be pursuing. Furthermore, COFs-based metal-free heterojunctions reveal great potentials in organic photocatalytic reaction, e.g., artificial photosynthesis and photocatalytic aerobic oxidation.<sup>[24,33]</sup>

#### 4.3. Insufficient Knowledge of Reaction Mechanisms

Although the structure of COFs materials can be precisely predicted, the accurate synthesis condition of COFs often heavily relies on trial and error, and it is even more challenge to synthesize target materials in a precise manner when combined with other non-metallic components. Theoretical calculations and new methodologies like artificial intelligence machine learning can be utilized to assist in designing highly effective COFs-based metal-free heterojunctions. Data-driven screening procedure, based on a COFs heterojunction database, opens up new avenues, and inspires the development of COFs-based metal-free heterojunction photocatalysts.<sup>[109]</sup>

Apart from the synthesis reaction mechanism, certain fundamental principles, e.g., the concrete implementation of synergistic effects and catalytic reaction mechanisms still require in-depth investigation. Reliable characterization supplemented by relevant theoretical calculations, is desirable. Currently, characterizations mainly rely on indirect technologies such as photoluminescence spectrum, time-resolved photoluminescence, photocurrent and impedance tests to evaluate photogenerated charge behaviors, electron spin resonance and capture experiments to confirm active species, and SEM/AFM/TEM combined with XPS and N<sub>2</sub> adsorption-desorption to evaluate surface active sites. However, these technologies lack direct evidence to confirm active intermediates indeed participate in surface redox reactions. To acquire direct evidence for elucidating the surface redox reactions in real-time, in situ technologies (in situ extended X-ray absorption fine structure, in-situ XPS/Raman/FTIR, etc.) that integrate powerful real-time experiments phenomena is highly demand, which would enable us to deeply understand the underlying reaction mechanism and guide the design of target photocatalysts. For example, in-site FTIR and in-site Roman were utilized to real-time monitors changes in functional group of intermediates and the adsorption/degradation processes on the surface of photocatalysts.

#### 4.4. Non-Standardized Reported Photocatalytic Activities

The comparability of photocatalytic activities reported by different research groups is influenced by various specific details in the experimental set-up, including detection methods, light wavelength/intensity, filter usage, type/concentration of co-catalyst/sacrificial-agent, concentration of sample/substrate, temperature, pressure and so on. Literatures suggest standardizing (3D-printable) photoreactor setups,<sup>[110]</sup> and reporting AQY or SCC alongside generation rates for improved consistency.<sup>[2]</sup>

#### Acknowledgements

This work was supported by the Natural Science Foundation Project of Jilin Province (20240601037RC, 20230101297JC, YDZJ202201ZYTS347,

YDZJ202102CXJD049), and the Project of Jilin Province Development and Reform Commission (2023C032-5, 2023C032-4, 2023C032-2).

#### Conflict of Interest

The authors declare no conflict of interest.

#### Keywords

covalent organic frameworks, heterojunction, metal-free, photocatalysis

Received: May 31, 2024

Revised: July 26, 2024

Published online:

- [1] J. Chen, D. Yuan, Y. Wang, *Adv. Funct. Mater.* **2023**, *33*, 2304071.
- [2] Y. Wang, A. Vogel, M. Sachs, R. S. Sprick, L. Wilbraham, S. J. A. Moniz, R. Godin, M. A. Zwijnenburg, J. R. Durrant, A. I. Cooper, J. Tang, *Nat. Energy* **2019**, *4*, 746.
- [3] K. Chen, A. Cai, T. T. Li, *ChemSusChem* **2023**, *16*, 202300021.
- [4] T. He, Y. Zhao, *Angew. Chem., Int. Ed.* **2023**, *62*, 202303086.
- [5] A. Fujishima, K. Honda, *Nature* **1972**, *238*, 37.
- [6] W. Wang, X. Wang, M. Gao, Z. Li, W. Zhou, *Coordin. Chem. Rev.* **2024**, *506*.
- [7] M. Zhang, M. Lu, Z. L. Lang, J. Liu, M. Liu, J. N. Chang, L. Y. Li, L. J. Shang, M. Wang, S. L. Li, Y. Q. Lan, *Angew. Chem., Int. Ed.* **2020**, *59*, 6562.
- [8] Z. Zhou, Y. Xiao, J. Tian, N. Nan, R. Song, J. Li, *J. Mater. Chem. A* **2023**, *11*, 3245.
- [9] S. Qi, R. Guo, Z. Bi, Z. Zhang, C. Li, W. Pan, *Small* **2023**, *19*, 2303632.
- [10] T. Banerjee, F. Podjaski, J. Kröger, B. P. Biswal, B. V. Lotsch, *Nat. Rev. Mater.* **2020**, *6*, 168.
- [11] V. S. Vyas, V. Lau, B. V. Lotsch, *Chem. Mater.* **2016**, *28*, 5191.
- [12] Y. Zhang, C. Guo, L. Zhou, X. Yao, Y. Yang, H. Zhuang, Y.-R. Wang, Q. Huang, Y. Chen, S.-L. Li, Y.-Q. Lan, *Small Sci.* **2023**, *3*, 2300056.
- [13] G. Yan, X. Sun, Y. Zhang, H. Li, H. Huang, B. Jia, D. Su, T. Ma, *Nano-Micro Lett.* **2023**, *15*, 132.
- [14] A. P. Côté, A. I. Benin, N. W. Ockwig, M. O'Keeffe, A. J. Matzger, O. M. Yaghi, *Science* **2005**, *310*, 1166.
- [15] Z. Wang, S. Zhang, Y. Chen, Z. Zhang, S. Ma, *Chem. Soc. Rev.* **2020**, *49*, 708.
- [16] Q. Zhang, P. Zhi, J. Zhang, S. Duan, X. Yao, S. Liu, Z. Sun, S. C. Jun, N. Zhao, L. Dai, L. Wang, X. Wu, Z. He, Q. Zhang, *Adv. Mater.* **2024**, *36*, 2313152.
- [17] M. B. Asif, S. Kim, T. S. Nguyen, J. Mahmood, C. T. Yavuz, *J. Am. Chem. Soc.* **2024**, *146*, 3567.
- [18] X. Liu, D. Huang, C. Lai, G. Zeng, L. Qin, H. Wang, H. Yi, B. Li, S. Liu, M. Zhang, R. Deng, Y. Fu, L. Li, W. Xue, S. Chen, *Chem. Soc. Rev.* **2019**, *48*, 5266.
- [19] N. Singh, M. Won, J. An, C. Yoon, D. Kim, S. Joong Lee, H. Kang, J. Seung Kim, *Coordin. Chem. Rev.* **2024**, *506*, 215720.
- [20] Y. R. Wang, H. M. Ding, X. Y. Ma, M. Liu, Y. L. Yang, Y. Chen, S. L. Li, Y. Q. Lan, *Angew. Chem., Int. Ed.* **2021**, *61*, 202114648.
- [21] J. N. Chang, Q. Li, J. W. Shi, M. Zhang, L. Zhang, S. Li, Y. Chen, S. L. Li, Y. Q. Lan, *Angew. Chem., Int. Ed.* **2023**, *62*, 202218868.
- [22] J. N. Chang, Q. Li, Y. Yan, J. W. Shi, J. Zhou, M. Lu, M. Zhang, H. M. Ding, Y. Chen, S. L. Li, Y. Q. Lan, *Angew. Chem., Int. Ed.* **2022**, *61*, 202209289.
- [23] L. Qin, C. Ma, J. Zhang, T. Zhou, *Adv. Funct. Mater.* **2024**, 2401562.
- [24] H. Chen, H. S. Jena, X. Feng, K. Leus, P. Van Der Voort, *Angew. Chem., Int. Ed.* **2022**, *61*, 202204938.

- [25] T. Li, J. Shi, Z. Liu, W. Xie, K. Cui, B. Hu, G. Che, L. Wang, T. Zhou, C. Liu, *Catal. Sci. Technol.* **2022**, 12, 4591.
- [26] X. Zhao, P. Pachfule, A. Thomas, *Chem. Soc. Rev.* **2021**, 50, 6871.
- [27] Y. Liu, J. Li, J. Lv, Z. Wang, J. Suo, J. Ren, J. Liu, D. Liu, Y. Wang, V. Valtchev, S. Qiu, D. Zhang, Q. Fang, *J. Am. Chem. Soc.* **2023**, 145, 9679.
- [28] J. Li, D. Zhao, J. Liu, A. Liu, D. Ma, *Molecules* **2020**, 25, 2425.
- [29] H. Dai, H. Li, Q. Yang, *Micropor. Mesopor. Mat.* **2022**, 342, 112121.
- [30] X. Wang, L. Chen, S. Y. Chong, M. A. Little, Y. Wu, W.-H. Zhu, R. Clowes, Y. Yan, M. A. Zwijnenburg, R. S. Sprick, A. I. Cooper, *Nat. Chem.* **2018**, 10, 1180.
- [31] J. Wang, Y. Yu, J. Cui, X. Li, Y. Zhang, C. Wang, X. Yu, J. Ye, *Appl. Catal. B Environ.* **2022**, 301, 120814.
- [32] Y. Liu, Y. Wang, J. Shang, J. Peng, T. Zhu, *Appl. Catal. B Environ.* **2024**, 350, 123937.
- [33] M.-Y. Yang, S.-B. Zhang, M. Zhang, Z.-H. Li, Y.-F. Liu, X. Liao, M. Lu, S.-L. Li, Y.-Q. Lan, *J. Am. Chem. Soc.* **2024**, 146, 3396.
- [34] J.-P. Liao, M. Zhang, P. Huang, L.-Z. Dong, T.-T. Ma, G.-Z. Huang, Y.-F. Liu, M. Lu, S.-L. Li, Y.-Q. Lan, *ACS Catal.* **2024**, 14, 3778.
- [35] Y. Ma, Y. Fu, W. Jiang, Y. Wu, C. Liu, G. Che, Q. Fang, *J. Mater. Chem. A* **2022**, 10, 10092.
- [36] Y. Yao, Y. Han, S. Qi, D. Sun, J. Lang, B. Hu, Y. Ma, C. Liu, *Int. J. Hydrogen Energy* **2024**, 63, 184.
- [37] Y. Ma, L. Shang, J. Li, Y. Wu, G. Che, C. Liu, Q. Fang, *Chem. Eng. J.* **2024**, 484, 149347.
- [38] N. Xu, Y. Liu, W. Yang, J. Tang, B. Cai, Q. Li, J. Sun, K. Wang, B. Xu, Q. Zhang, Y. Fan, *ACS Appl. Energy Mater.* **2020**, 3, 11939.
- [39] L. Wang, R. Lian, Y. Zhang, X. Ma, J. Huang, H. She, C. Liu, Q. Wang, *Appl. Catal. B Environ.* **2022**, 315, 121568.
- [40] L. Huang, J. Yang, Y. Asakura, Q. Shuai, Y. Yamauchi, *ACS Nano* **2023**, 17, 8918.
- [41] R. Liu, K. T. Tan, Y. Gong, Y. Chen, Z. Li, S. Xie, T. He, Z. Lu, H. Yang, D. Jiang, *Chem. Soc. Rev.* **2021**, 50, 120.
- [42] Q. Guan, L.-L. Zhou, Y.-B. Dong, *J. Am. Chem. Soc.* **2023**, 145, 1475.
- [43] H. Kim, N. Kim, J. Ryu, *Inorg. Chem. Front.* **2021**, 8, 4107.
- [44] S. Patial, P. Raizada, A. Aslam Parwaz Khan, A. Singh, Q. Van Le, V. Huy Nguyen, R. Selvasembian, C. Mustansar Hussain, P. Singh, *Chem. Eng. J.* **2022**, 433, 134594.
- [45] J. Jayakumar, H. H. Chou, *ChemCatChem* **2020**, 12, 689.
- [46] M. Z. Rahman, M. G. Kibria, C. B. Mullins, *Chem. Soc. Rev.* **2020**, 49, 1887.
- [47] J. Tang, Q. Li, Y. Liu, N. Xu, K. Wang, Q. Zhang, W. Yang, Y. Fan, *Int. J. Hydrogen Energy* **2021**, 46, 17666.
- [48] C. Nie, X. Wang, P. Lu, Y. Zhu, X. Li, H. Tang, *J. Mater. Sci. Technol.* **2024**, 169, 182.
- [49] B. Zhu, J. Sun, Y. Zhao, L. Zhang, J. Yu, *Adv. Mater.* **2023**, 36, 2310600.
- [50] Q. Xu, L. Zhang, B. Cheng, J. Fan, J. Yu, *Chem* **2020**, 6, 1543.
- [51] J. Fu, Q. Xu, J. Low, C. Jiang, J. Yu, *Appl. Catal. B Environ.* **2019**, 243, 556.
- [52] F. Li, G. Zhu, J. Jiang, L. Yang, F. Deng, X. Li, *J. Mater. Sci. Technol.* **2024**, 177, 142.
- [53] J. Zhang, L. Wang, M. Mousavi, J. B. Ghasemi, J. Yu, *Chin. J. Struct. Chem.* **2022**, 41, 2206003.
- [54] J. Zou, G. Liao, J. Jiang, Z. Xiong, S. Bai, H. Wang, P. Wu, P. Zhang, X. Li, *Chin. J. Struct. Chem.* **2022**, 41, 2201025.
- [55] M. Liu, F. Zhao, Y. Chu, J. Zhao, F. Meng, Y. Han, *Chem. Eng. Sci.* **2024**, 288, 119827.
- [56] Y. Liu, L. Jiang, Y. Tian, Z. Xu, W. Wang, M. Qiu, H. Wang, X. Li, G. Zhu, Y. Wang, *Inorg. Chem.* **2023**, 62, 3271.
- [57] X. Song, Y. Wu, X. Zhang, X. Li, Z. Zhu, C. Ma, Y. Yan, P. Huo, G. Yang, *Chem. Eng. J.* **2021**, 408, 127292.
- [58] Z. Jin, Q. Zhang, J. Chen, S. Huang, L. Hu, Y.-J. Zeng, H. Zhang, S. Ruan, T. Ohno, *Appl. Catal. B Environ.* **2018**, 234, 198.
- [59] J. Liang, W. Li, J. Chen, X. Huang, Y. Liu, X. Zhang, W. Shu, B. Lei, H. Zhang, *J. Mater. Chem. A* **2022**, 10, 23384.
- [60] A. Deng, Y. Sun, Z. Gao, S. Yang, Y. Liu, H. He, J. Zhang, S. Liu, H. Sun, S. Wang, *Nano Energy* **2023**, 108, 108228.
- [61] X. Yue, J. Fan, Q. Xiang, *Adv. Funct. Mater.* **2021**, 32, 2110258.
- [62] L. Chen, J. T. Ren, Z. Y. Yuan, *Adv. Energy Mater.* **2023**, 13, 2203720.
- [63] P. Dong, A. Zhang, T. Cheng, J. Pan, J. Song, L. Zhang, R. Guan, X. Xi, J. Zhang, *Chin. J. Catal.* **2022**, 43, 2592.
- [64] W. Si, J. Yang, Y. Cao, W. Qin, *J. Alloy. Compd.* **2023**, 968, 172218.
- [65] C. Wang, F. Zheng, L. Zhang, J. Yang, P. Dong, *Appl. Surf. Sci.* **2023**, 640, 158383.
- [66] X.-L. Song, L. Chen, L.-J. Gao, J.-T. Ren, Z.-Y. Yuan, *Green Energy Environ.* **2024**, 9, 166.
- [67] S. Tao, S. Wan, Q. Huang, C. Li, J. Yu, S. Cao, *Chin. J. Struct. Chem.* **2022**, 41, 2206048.
- [68] X. Wang, K. Maeda, A. Thomas, K. Takanabe, G. Xin, J. M. Carlsson, K. Domen, M. Antonietti, *Nat. Mater.* **2008**, 8, 76.
- [69] Q. Zhang, W. Gong, H. Che, B. Liu, Y. Ao, *Chin. J. Struct. Chem.* **2023**, 42, 100205.
- [70] M. Luo, Q. Yang, K. Liu, H. Cao, H. Yan, *Chem. Commun.* **2019**, 55, 5829.
- [71] M. Luo, Q. Yang, W. Yang, J. Wang, F. He, K. Liu, H. Cao, H. Yan, *Small* **2020**, 16, 2001100.
- [72] Y. Xing, L. Yin, Y. Zhao, Z. Du, H.-Q. Tan, X. Qin, W. Ho, T. Qiu, Y.-G. Li, *ACS Appl. Mater. Interfaces* **2020**, 12, 51555.
- [73] C. Lin, C. Han, L. Gong, X. Chen, J. Deng, D. Qi, Y. Bian, K. Wang, J. Jiang, *Catal. Sci. Technol.* **2021**, 11, 2616.
- [74] Y. Hou, C.-X. Cui, E. Zhang, J.-C. Wang, Y. Li, Y. Zhang, Y. Zhang, Q. Wang, J. Jiang, *Dalton Trans.* **2019**, 48, 14989.
- [75] H. Hu, Y. Hu, W. Kong, Y. Tao, Q. Jiang, J. Wang, C. Li, H. Xie, Y. Shi, Y. Li, G. Chen, J. Liang, S. Zhou, Y. Kong, Y. Zhu, *J. Environ. Chem. Eng.* **2023**, 11, 111108.
- [76] Y. Yao, Y. Hu, H. Hu, L. Chen, M. Yu, M. Gao, S. Wang, *J. Colloid Interf. Sci.* **2019**, 554, 376.
- [77] J. Jiang, S. Zhou, Z. Chen, P. Gu, Y. Li, Q. Xu, *New J. Chem.* **2023**, 47, 7538.
- [78] Y. Cao, R. Wu, Y. Zhou, D. Jiang, W. Zhu, *Adv. Funct. Mater.* **2022**, 32, 2203005.
- [79] S. Zhong, Y. Wang, S. Li, S. Wang, X. Que, L. Sheng, J. Peng, L. Zhao, L. Yuan, M. Zhai, *Sep. Purif. Technol.* **2022**, 294, 121204.
- [80] C. M. Aitchison, Y. Zhang, W. Lu, I. McCulloch, *Faraday Discuss.* **2024**, 250, 251.
- [81] P. Bika, I. Papailias, T. Giannakopoulou, C. Tampaxis, T. A. Steriotis, C. Trapalis, P. Dallas, *Catalysts* **2023**, 13, 1331.
- [82] H. Wang, E. Almatrafi, Z. Wang, Y. Yang, T. Xiong, H. Yu, H. Qin, H. Yang, Y. He, C. Zhou, G. Zeng, P. Xu, *J. Colloid Interf. Sci.* **2022**, 608, 1051.
- [83] A. E. Hassan, A. M. Elewa, M. S. A. Hussien, A. F. M. El-Mahdy, I. M. A. Mekhemer, I. S. Yahia, T. A. Mohamed, H.-H. Chou, Z. Wen, *J. Colloid Interf. Sci.* **2024**, 653, 1650.
- [84] J. Zhou, M. Dong, Y. Sun, G.-G. Shan, C.-Y. Sun, S.-Q. You, X.-L. Wang, Z.-H. Kang, Z.-M. Su, *ACS Appl. Mater. Interfaces* **2022**, 14, 6476.
- [85] J. Guo, D. Ma, F. Sun, G. Zhuang, Q. Wang, A. M. Al-Enizi, A. Nafady, S. Ma, *Sci. China Chem.* **2022**, 65, 1704.
- [86] J. Ding, Y. Lou, G. Dong, Y. Zhang, *J. Photoch. Photobio. A* **2023**, 439, 114590.
- [87] Q. Wu, M. J. Mao, Q. J. Wu, J. Liang, Y. B. Huang, R. Cao, *Small* **2020**, 17, 2004933.
- [88] W. Hao, C. Sui, G. Cheng, J. Li, L. Miao, G. Zhao, Y. Sang, J. Li, C. Zhao, Y. Zhou, Z. Zang, Y. Zhao, X. He, C. Wang, *ACS Nano* **2024**, 18, 10485.
- [89] Y.-H. Yao, J. Li, H. Zhang, H.-L. Tang, L. Fang, G.-D. Niu, X.-J. Sun, F.-M. Zhang, *J. Mater. Chem. A* **2020**, 8, 8949.

- [90] V. N. Gopalakrishnan, D.-T. Nguyen, J. Becerra, M. Sakar, J. M. E. Ahad, J. J. Jautzy, L. M. Mindorff, F. Béland, T.-O. Do, *ACS Appl. Energy Mater.* **2021**, 4, 6005.
- [91] Y. Yang, Q. Guo, Q. Li, L. Guo, H. Chu, L. Liao, X. Wang, Z. Li, W. Zhou, *Adv. Funct. Mater.* **2024**, 34, 2400612.
- [92] Y. Cong, X. Li, S. Zhang, Q. Zheng, Y. Zhang, S.-W. Lv, *ACS Appl. Mater. Interfaces* **2023**, 15, 43799.
- [93] X. Xu, Y. Yue, G. Xin, N. Huang, *Macromol. Rapid. Commun.* **2022**, 44, 2200715.
- [94] Y.-O. He, Y.-M. Fu, X. Meng, L. Xue, R.-G. Yang, J.-X. Qu, Z.-M. Su, H.-N. Wang, *Appl. Catal. A-Gen.* **2023**, 663, 119320.
- [95] Y. Yang, C. Schäfer, K. Börjesson, *Chem* **2022**, 8, 2217.
- [96] H. Xue, Z. Bi, J. Cheng, S. Xiong, Y. Wang, *Ind. Eng. Chem. Res.* **2021**, 60, 8687.
- [97] L. Yao, A. Rodriguez-Camargo, M. Xia, D. Mucke, R. Guntermann, Y. Liu, L. Grunenberg, A. Jimenez-Solano, S. T. Emmerling, V. Duppel, K. Sivula, T. Bein, H. Qi, U. Kaiser, M. Gratzel, B. V. Lotsch, *J. Am. Chem. Soc.* **2022**, 144, 10291.
- [98] M. Deng, J. Guo, X. Ma, Y. Fu, H. Du, D. Hao, Q. Wang, *Sep. Purif. Technol.* **2023**, 326, 124786.
- [99] Z. Liang, R. Shen, P. Zhang, Y. Li, N. Li, X. Li, *Chin. J. Catal.* **2022**, 43, 2581.
- [100] J. Tang, Y. Chen, T. Gong, J. Gong, *ACS Macro Lett.* **2023**, 12, 1564.
- [101] Y. Yang, W. Zhao, H. Niu, Y. Cai, *ACS Appl. Mater. Interfaces* **2021**, 13, 42035.
- [102] M. Yan, F. Jiang, Y. Wu, *Int. J. Hydrogen Energy* **2023**, 48, 8867.
- [103] Q. Wu, M.-J. Mao, Q.-J. Wu, J. Liang, Y.-B. Huang, R. Cao, *Small* **2021**, 17, 2004933.
- [104] L. Yao, Y. Zhang, H.-X. Wang, Y. Guo, Z.-M. Zhuang, W. Wen, X. Zhang, S. Wang, *J. Mater. Chem. A* **2020**, 8, 8518.
- [105] Z. Yong, T. Ma, *Angew. Chem., Int. Ed.* **2023**, 62, 202308980.
- [106] L. Li, L. Xu, Z. Hu, J. C. Yu, *Adv. Funct. Mater.* **2021**, 31, 2106120.
- [107] J. N. Chang, J. W. Shi, Q. Li, S. Li, Y. R. Wang, Y. Chen, F. Yu, S. L. Li, Y. Q. Lan, *Angew. Chem., Int. Ed.* **2023**, 62, 202303606.
- [108] P. Zhang, Z. Wang, S. Wang, J. Wang, J. Liu, T. Wang, Y. Chen, P. Cheng, Z. Zhang, *Angew. Chem., Int. Ed.* **2022**, 61, 202213247.
- [109] L. Sheng, J. Wang, W. Zhang, Q. Li, J. Yang, *J. Phys. Chem. Lett.* **2023**, 14, 9207.
- [110] C. C. Le, M. K. Wismer, Z.-C. Shi, R. Zhang, D. V. Conway, G. Li, P. Vachal, I. W. Davies, D. W. C. MacMillan, *ACS Cent. Sci.* **2017**, 3, 647.



**Tianyu Zhou** received her Ph.D. degree in 2018 from Jilin University, China. She became an associate professor at Jilin Normal University in 2022. Her current research interests focus on covalent organic frameworks, carbon nitride and other metal-free based photocatalytic materials in clean energy production and environmental water remediation.



**Yunchao Ma** obtained her Ph.D. degree in 2020 from Jilin University, China. She is now a lecturer at Jilin Normal University. Her research interests are in the structural design and properties of covalent organic frameworks, including photocatalytic water splitting and photocatalytic nitrogen reduction.



**Hao Feng** is currently pursuing his Ph.D. degree under the supervision of professor Chunbo Liu at Jilin Normal University, China. His research interests focus on covalent organic frameworks, organic photovoltaic devices and electrocatalytic organic conversion.



**Ye Lu** is currently pursuing his Ph.D. degree under the supervision of professor Guangbo Che and professor Chunbo Liu at Jilin Normal University, China. His current research interests focus on the photocatalytic removal of antibiotic resistant bacteria and antibiotic resistance genes.



**Guangbo Che** received his Ph.D. in Changchun Institute of Optics, Fine Mechanics and Physics, Chinese Academy of Sciences, in 2006. As a professor in Baicheng Normal University, he focuses on covalent organic frameworks, inorganic-organic hybrid materials and their application in photoelectrocatalysis.



**Chunbo Liu** received her Ph.D. degree in Changchun Institute of Optics, Fine Mechanics and Physics, Chinese Academy of Sciences, in 2007. As a professor in Jilin Normal University, her research interests encompass covalent organic frameworks, inorganic-organic hybrid materials and their application in photoelectrocatalysis.



**Yaqian Lan** received his B.S. and Ph.D. degrees (2009) from Northeast Normal University under the supervision of Prof. Zhong-Min Su. In 2010, he joined the National Institute of Advanced Industrial Science and Technology (AIST, Japan) as a JSPS postdoctoral fellow. In 2012, he became a professor of chemistry at Nanjing Normal University (NNU, China). In 2021, he joined South China Normal University (SCNU, China) as a professor of chemistry. His current research interest focuses on the synthesis of new crystalline materials and catalytic research related to clean energy applications.